

Review

# Fluorescent Sensors for Detecting and Imaging Metal Ions in Biological Systems: Recent Advances and Future Perspectives

Yang Shi <sup>1</sup>, Wenxian Zhang <sup>1</sup>, Yi Xue <sup>1</sup> and Jingjing Zhang <sup>1,2,\*</sup> 

<sup>1</sup> Key Laboratory of Analytical Chemistry for Life Science, School of Chemistry and Chemical Engineering, Nanjing University, Nanjing 210023, China

<sup>2</sup> Chemistry and Biomedicine Innovation Center (ChemBIC), Nanjing University, Nanjing 210023, China

\* Correspondence: jing15209791@nju.edu.cn

**Abstract:** Metal ions play a crucial role in many biochemical processes, and when in a state of scarcity or surplus, they can lead to various diseases. Therefore, the development of a selective, sensitive, cost-effective, and fast-responding sensor to detect metal ions is critical for in vitro medical diagnostics. In recent years, fluorescent sensors have been extensively investigated as potent kits for the effective assessment of metal ions in living systems due to their high sensitivity, selectivity, ability to perform real-time, non-invasive monitoring, and versatility. This review is an overview of recent advances in fluorescent sensors for the detection and imaging of metal ions in biosystems from 2018 to date. Specifically, we discuss their application in detecting essential metal ions and non-essential metal ions for in vitro diagnostics, living cell imaging, and in vivo imaging. Finally, we summarize remaining challenges and offer a future outlook on the above topics.

**Keywords:** fluorescent sensors; metal ions; biosystems; detection; imaging



**Citation:** Shi, Y.; Zhang, W.; Xue, Y.; Zhang, J. Fluorescent Sensors for Detecting and Imaging Metal Ions in Biological Systems: Recent Advances and Future Perspectives. *Chemosensors* **2023**, *11*, 226. <https://doi.org/10.3390/chemosensors11040226>

Academic Editor: Ambra Giannetti

Received: 2 March 2023

Revised: 1 April 2023

Accepted: 4 April 2023

Published: 6 April 2023



**Copyright:** © 2023 by the authors. Licensee MDPI, Basel, Switzerland. This article is an open access article distributed under the terms and conditions of the Creative Commons Attribution (CC BY) license (<https://creativecommons.org/licenses/by/4.0/>).

## 1. Introduction

Metal ions are known to play indispensable roles in many critical biochemical processes. The amount and dispersion of metal ions in body fluids have a significant impact on the normal physiological function of the human body. In terms of their effects in biosystems, the general public generally classifies metals into two categories: essential and non-essential. Currently, it is widely recognized that there are ten essential metal ions for life, and our body must have appropriate amounts of them [1–4], including potassium (K), sodium (Na), calcium (Ca), magnesium (Mg), cobalt (Co), molybdenum (Mo), iron (Fe), copper (Cu), zinc (Zn), and manganese (Mn). Among them, K, Na, Ca, and Mg make up over 99% of the total metal elements in the human body, while the remaining six elements are present in small amounts. When essential metal ions are maintained at normal levels (Table 1), they play a crucial role in various physiological functions, including catalyzing enzymes, participating in oxidative metabolism, and contributing to DNA synthesis [5–7]. Their absence or disruption of homeostasis can lead to various diseases and health disorders. On a different note, non-essential metal ions, such as mercury (Hg), silver (Ag), gold (Au), and lead (Pb), are often harmful to human health. They are not easily biodegraded and can accumulate in the human body through the biological amplification of the food chain. These non-essential metal ions can react with and deactivate proteins and enzymes in the human body, leading to chronic poisoning. It is important to note that the distinction between essential and non-essential metal ions is somewhat relative, as even essential metal ions can become toxic if their concentrations become too high [8]. Therefore, a selective, facile, sensitive, cost-effective, and fast-responding sensor to detect metal ions is of great significance for in vitro healthcare diagnostics and biological system imaging.

**Table 1.** Normal level range of essential metal ions commonly found in biological systems.

Analytes	Normal Level Range in Biological System	Reference
Na <sup>+</sup>	135–145 mM (serum)	[9–11]
K <sup>+</sup>	3.5–5.4 mM (serum), 19–66 mM (urea)	[12,13]
Ca <sup>2+</sup>	10–6 M (intracellular), 10–3 M (extracellular fluid)	[14]
Mg <sup>2+</sup>	0.65–1.05 mM (serum)	[15]
Cu <sup>2+</sup>	1.4–2.1 mg/kg (adult human body)	[16]
Zn <sup>2+</sup>	12–16 μM (serum)	[17]
Fe <sup>3+</sup>	14–32 μM (serum)	[18]

Over the last few decades, various traditional analytical methods have been developed to measure metal ions, including inductively coupled plasma mass spectrometry (ICP-MS) [19], inductively coupled plasma–atomic/optical emission spectrometry [20], atomic absorption spectrophotometry (AAS) [21], and flame atomic absorption spectrometry (FAAS) [22]. However, these methods often require costly equipment, trained operators, and complex sample preparation, rendering detection in the field and in real time difficult to achieve. To address these limitations, fluorescent sensors for metal ion detection have gained significant interest due to their high selectivity and sensitivity, ease of use, low cost, and relatively short response time [6,23–25]. In addition, as a versatile enabling tool with excellent biocompatibility, the fluorescent sensor enables simultaneous and non-invasive imaging of metal ion distribution in biological systems in real time [6]. As a result, fluorescent sensors have greatly contributed to our understanding of the generation, positioning, transport, and bio-role of metal ions in complex living systems.

The last decade has seen unprecedented advances in the techniques of fluorescent sensors. In addition, considerable progress has been achieved in the exploitation of fluorescent probes with organic fluorescent dyes, benefiting from new fluorescent imaging techniques because of their good biocompatibility, high spatiotemporal resolution, and accessibility to chemical modifications. These features allow for the monitoring of the cellular localization and dynamics of many of the biotargets. Although many reviews have been published regarding fluorescent sensors that detect small molecules, including carbonyl species [26], sulfite derivatives [27], glutathione [28,29], hydrogen peroxide [30], peroxynitrite [31], and metal ions [32,33], only a few reviews have covered the advancement of metal ion sensors in biological systems in detail. To fill this gap, we here provide a comprehensive review that covers recent progress in metal ion sensors in the past five years, including reaction-based, nucleic acid-based, and material-based sensors. We discuss their application in detecting metal ions, including monovalent, divalent, and other metal ions, for in vitro diagnostics, living cell imaging, and in vivo imaging. Finally, we outline the current limitations and future directions in these areas.

## 2. Categorization of Fluorescent Sensors for Metal Ions

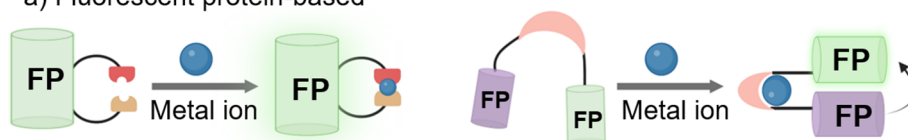
Numerous metal-ion sensors have been explored in the past five years. Despite some ambiguity in the literature regarding these terms, we are guided by the widely accepted consensus to divide new metal ion sensing systems into four categories, which are genetically encoded biosensors, molecular probes, chemosensors, and nanosensors.

Genetically encoded biosensors consist of sensing elements and transduction elements. The sensing element is used to receive input messages, which may come from metabolites, chemistry, or the environment, and the transduction element converts the inputs to an output signal, usually fluorescent [34]. There are different kinds of genetically encoded biosensors, among which the most widely used in metal ion detection are fluorescent protein-based biosensors [35] and nucleic acid-based biosensors [36]. Fluorescent protein-based biosensors utilize a peptide or protein domain that functions as a metal binding site (Figure 1A(a)). For single fluorescent protein-based sensors, upon metal ion binding, a change occurs in the chemical or electronic environment surrounding the chromophore, resulting in either a shift in the excitation or emission spectrum or a change in intensity [37,38].

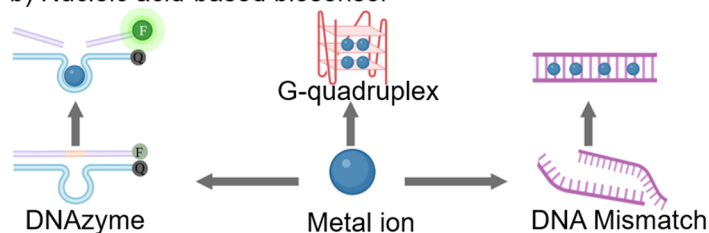
In biosensors with two fluorescent proteins, fluorescent resonance energy transfer (FRET) is utilized to detect metal binding-induced conformational changes or protein-protein interactions. To detect metal ions in living systems, fluorescent protein-based biosensors are commonly used. However, this biosensor is not ideal for *in vitro* detection due to its reliance on a highly stable intracellular environment.

## A Genetically encoded biosensor

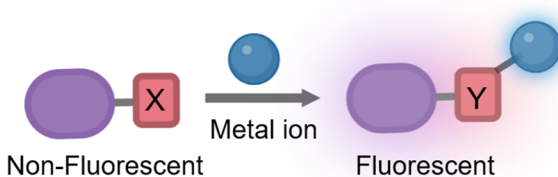
### a) Fluorescent protein-based



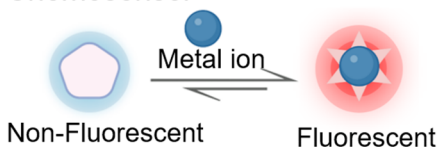
### b) Nucleic acid-based biosensor



## B Molecular probe



## C Chemosensor



## D Nanosensor

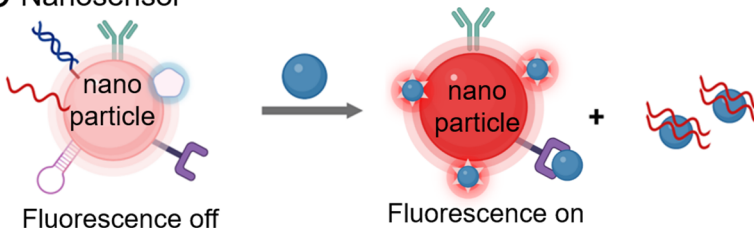


**Figure 1.** Schematic representation of genetically encoded biosensors, molecular probes, chemosensors, and nanosensors. An emission turn-on response is shown as an exemplary signal response to the presence of an analyte. (A) Genetically encoded biosensors: (a) fluorescent protein-based biosensors; (b) nucleic acid-based biosensors; (B) molecular probes; (C) chemosensors; (D) nanosensors.

In contrast, the sensing element of nuclear acid-based sensors is usually designed based on functional nucleic acids (FNA) [36,39] and DNA mismatch [40] (Figure 1A(b)). Two primary types of functional DNA have been developed for metal sensing: G-quadruplex (GQ) [41] and DNAzymes [42], which has a number of desirable properties to detect metal ions [43]. First, FNAs are critically separated from a large DNA library containing  $10^{14}$ – $10^{15}$  DNA molecules, which means that they are extremely selective. Second, DNA can be produced from any designed nucleotide sequence and is easily functionalized with the required chemical tags. Third, DNA is highly stable and can be denatured

multiple times before apparently losing its binding activity to metal ions. Finally, FNAs do not require the deliberate design of metal binding sites, which are indispensable for fluorescent protein-based biosensors. Moreover, genetically encoded DNA-based optical sensors can be assembled continuously and efficiently through carefully designed DNA sequences to generate signal amplification strategies such as hybrid chain reactions (HCR), thus improving sensitivity and reducing detection limits. Therefore, genetically encoded biosensors are widely used in metal ion biosensors and biological imaging *in vitro* and *in vivo*.

Molecular probes are systems that form strong, largely irreversible bonds with their target analytes (Figure 1B). These specific interactions often result in a distinct optical response, such as fluorescence emission or changes in absorbance bands [44]. Typically, molecular probes are covalently bonded to their targets through organic reaction mechanisms, allowing them to exhibit optical signals for *in vivo* imaging. In recent years, molecular probes have been extensively developed because of their higher sensitivity, improved detection accuracy, and relative simplicity of operation [45]. Particularly, they have attracted great interest in the field of ion detection and have become promising tools for visualizing ion migration, distribution, and concentration changes in biological systems [46–49].

Chemosensors reversibly bind metal ions in a reactive manner via a combination of non-covalent binding interactions with the analyte in a selective and reversible manner, and then alter one or more characteristics of the system in the form of color, fluorescence, or redox potential (Figure 1C). The kinetics of binding and unbinding are frequently rapid on the experimental/assay time scale, and the selection of the chromophore has a dramatic effect with respect to these features. In recent years, two major classes of organic dyes have been incorporated into organic molecule-based chemosensors as signal-reporting units, including classic organic dyes and new organic dyes with aggregation-induced emission (AIE). The former become quenched at higher concentrations or in the aggregated state, such as BODIPY [50], porphyrins [51], coumarins [52], naphthalimides [53], and rhodamines [54]. In contrast, the AIE dyes are strongly emitted in the aggregate or solid-state [55]. These unique fluorescent properties give fluorescent chemosensors remarkable capabilities in monitoring biologically relevant species *in vitro* and/or *in vivo*. Therefore, the exploitation of fluorescent chemosensors for the sensing of metal ions has become a highly active area of research.

Nanosensors are small-scale sensing devices with dimensions in the nanometer range, which are small yet powerful tools (Figure 1D). These sensors boast high sensitivity, making them ideal for the detection of low concentrations of target analytes in various fields [56–58], including environmental monitoring, medical diagnosis, food and beverage analysis, and industrial process control. In the design of nanosensors, the selection of the recognition element is crucial, as it determines the specificity and sensitivity of nanosensors. This element may take the form of a specific antibody, aptamer, or small molecule that is selectively bound to the metal ion of interest [59]. Moreover, nanosensors can be fabricated from a range of materials, including organic molecules, inorganic materials, and biomolecules. At the same time, the choice of material depends on the desired properties of the sensor, such as biocompatibility, stability, and sensitivity. One of the greatest advantages of nanosensors is their ability to simultaneously detect multiple metal ions in a single assay. This feature provides researchers with a complete picture of the status of metal ions in biological systems and allows them to make informed decisions based on the data. Furthermore, the recent advances in nanotechnology have enhanced the versatility and power of nanosensors, making them vital for the measurement of metal ions in complex environments.

### 3. In Vitro Detection of Metal Ions

The presence and distribution of various metal ions in human body fluids, such as blood, sweat, and urine, have a critical impact on human health [60–62]. Hence, *in vitro* detection of these metal ions through analysis of human body fluid samples plays a crucial role in disease prevention and early detection. Blood was previously the most common

type of sample taken as part of a routine physical examination. Recently, saliva, urine, and sweat have gained attention due to their abundant presence, diagnostic ability, and non-invasive sample extraction.

### 3.1. Fluorescent Sensors for Essential Metal Ions

#### 3.1.1. Na<sup>+</sup>

Sodium is considered to be the most common and critical metal ion in the environment and in biology [63]. High sodium levels are reflections of physiological disorders, such as hypertension and edema. In order to detect sodium ions, Liu and his co-workers obtained a mutant of the NaA43 DNAzyme through in vitro selection with a slightly acidic pH optimum and the same excellent specificity for Na<sup>+</sup> [64]. This makes it particularly useful for sodium sensing in environments such as the endosome and within cancer cells. Additionally, preliminary work has shown that this DNAzyme can detect sodium in serum, with a minimum detection threshold of 676 μM and a linear response at concentrations below 20 mM.

The Lu group developed a novel CRISPR-Cas12a-based sensor, employing a Na<sup>+</sup>-specific DNAzyme [65], as shown in Figure 2A. To link the DNAzyme recognition to Cas12a activation, the DNA activator was embedded in the DNAzyme sequences and labeled with biotin at the tail end. After Na<sup>+</sup>-catalyzed DNAzyme cleavage, the activation strand dissociates from the binding arm. Recognition of the activation strand by the Cas12a-crRNA complex triggers its trans-cleavage activity, which results in a turn-on fluorescence signal. The sensor has a detection limit of 0.10 mM, which is well below the sodium level normally found in human serum. Moreover, the sensor has been compared to a commercial sodium meter and found to be highly accurate (Figure 2B). Additionally, the Kaur group developed a highly selective fluorescent organic nanoparticle sensor based on Biginelli [66], which can measure Na<sup>+</sup> even in the presence of interfering K<sup>+</sup>. The sensor displayed a linear detection range of 0–25 μM and a minimum detection concentration of 22 nM. The practical applicability of this sensor has been demonstrated by successfully monitoring Na<sup>+</sup> concentrations in sweat samples from the lower back and urine samples.

#### 3.1.2. K<sup>+</sup>

Potassium is a vital cation for metabolic activity in living cells and is intimately mediated through a variety of cellular mechanisms. Li's team developed a transparent and stable G-2FPB-K<sup>+</sup> hydrogel for detecting K<sup>+</sup> [67]. The hydrogel is highly selective for K<sup>+</sup> and utilizes berberine to detect its formation during self-assembly. GQ is a unique nucleic acid structure consisting of a guanine-rich sequence with four helices formed by several stacked GQs [41]. Moreover, GQ manifests unique catalytic features upon interacting with hemin, a cofactor typically present in hemoproteins [68]. Given that the assembly of GQ requires cations, it could serve as a natural biosensor for specific cations. In another work, Cheng and co-workers created a K<sup>+</sup>-specific biosensor based on a dimerized GQ, whose enzymatic activity depends on the K<sup>+</sup> concentration [69]. When K<sup>+</sup> is available, the monomer, acted on by three G-quartets, will assemble into a dimer of six G-quartets. The sensor can detect K<sup>+</sup> selectively in the range of 1–200 mM, even in the presence of up to 140 mM Na<sup>+</sup> at ambient temperatures up to 45 °C.

Thioflavin T, or 4-(3,6-dimethyl-1,3-benzothiazol-3-ium-2-yl)-N,N-dimethylaniline chloride, first used to detect misfolded proteins, was later found to emit intense fluorescence emission when combined with GQ. Subsequently, Buranachai discovered that low concentrations of K<sup>+</sup> (25.0–500 nM) can reduce Thioflavin T fluorescence by replacing the dye in Thioflavin T-bimolecular GQ or Thioflavin T-tetramolecular GQ, as illustrated in Figure 2C [70]. Therefore, they developed a label-free turn-off fluorescent sensor for the detection of low K<sup>+</sup> concentrations. This simple and low-cost sensor only requires sample dilution and can be used with high accuracy for the direct detection of K<sup>+</sup> in normal urine samples, as shown in Figure 2D.

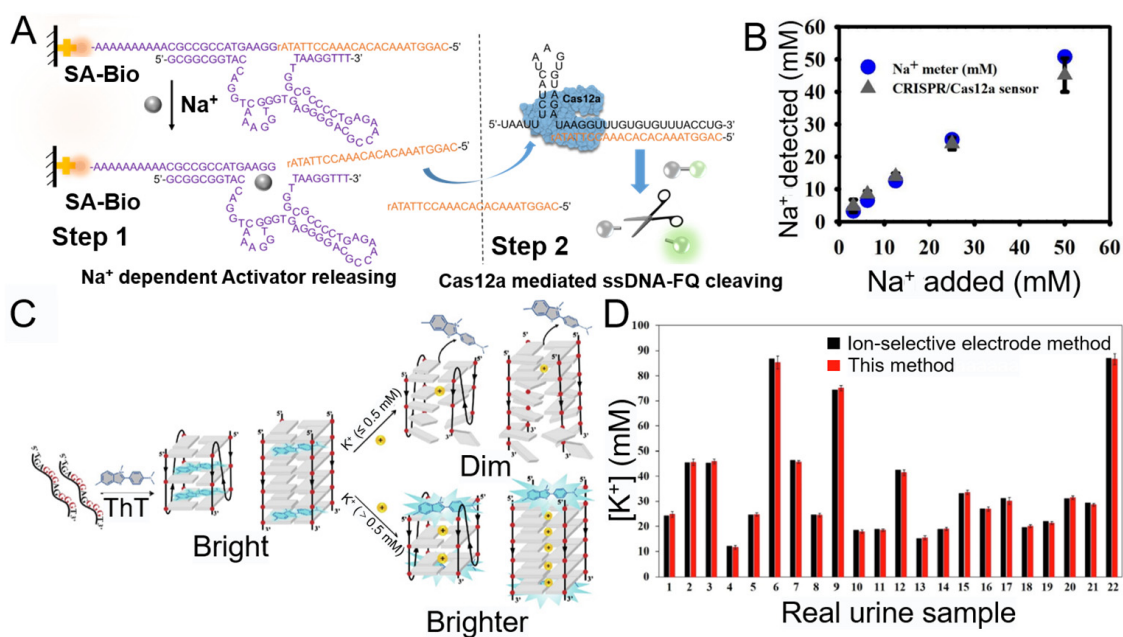


**Figure 2.** Two representative examples of essential metal ion detection in vitro: (A) Design and performance of NaA43 DNAzyme-regulated CRISPR-Cas12a sensor for Na<sup>+</sup> detection. (B) Comparison of a DNAzyme-regulated CRISPR/Cas12a sensor with a commercial Na<sup>+</sup> meter for different Na<sup>+</sup> concentration detection in human plasma. Reproduced from [65] with permission from the American Chemical Society, copyright 2020. (C) Proposed binding mechanism of Thioflavin T on the bimolecular GQ or the tetramolecular GQ formed by oligo-3-T under the influence of K<sup>+</sup>. (D) Comparison of K<sup>+</sup> concentrations in a real urine sample measured from the sensor and the reference values obtained from the ion-selective electrode (ISE) method used by the hospital. Reproduced from [70] with permission from Elsevier, copyright 2022.

### 3.1.3. Zn<sup>2+</sup>

Zinc is a vital micronutrient essential for numerous biological processes. Globally, approximately 20% of the human race is considered to be at risk for zinc scarcity, which can have a range of negative effects on growth, neurological function, reproduction, and the immune response. The high selectivity of DNAzyme for metal ions makes it a classical metal ion sensor. Despite the Zn<sup>2+</sup>-specific DNAzyme being first screened in 2009 [71], achieving in vitro detection of metal ions bound to biological macromolecules remains a major challenge. To address this limitation, Xing et al. developed a photocaged chelator, XDPAdCage, which can extract the Zn<sup>2+</sup> from the blood serum [72]. Upon 365 nm light irradiation, the chelated Zn<sup>2+</sup> was released into the buffer and finally quantified by 8–17 DNAzymes. The sensor showed high selectivity, accuracy, and reusability, demonstrating its potential for biological applications. On the other hand, the bioluminescent protein-based sensor is another attractive tool for Zn<sup>2+</sup> in complex media, such as blood serum. Merckx and colleagues developed two new bioluminescent sensor platforms that enable fast and accurate quantification of free Zn<sup>2+</sup> in serum [17]. In the first platform, the LuZi sensors use a modular design based on split NLuc complementation and BRET to a red fluorescent Cy3 dye, producing a strong shift from red to blue upon binding to Zn<sup>2+</sup>. The second platform, BLZinCh-Pro, replaces the long GGS linker with rigid polyproline linkers, resulting in four different sensor proteins with 3–4 times better emission ratios and Zn<sup>2+</sup> affinities. These sensors were applied for measuring cytosolic free Zn<sup>2+</sup> concentrations between 543 and 992 pM. Both sensors yielded similar results for free Zn<sup>2+</sup> concentration in (diluted) serum of 1–3 nM.

### 3.1.4. Cu<sup>2+</sup>

Copper (Cu) is an indispensable component of human life and is involved in various biological processes, including metalloprotein composition and gene expression. Wu's team synthesized a series of near-infrared (NIR) luminescent ruthenium complexes, which can be rapidly quenched by Cu<sup>2+</sup>, with remarkable selectivity for Cu<sup>2+</sup> detection in human serum [73]. In the same way, a new NIR BODIPY compound was reported by He et al. [74], which can be induced to undergo fluorescence bursts by Cu<sup>2+</sup>, while Mn<sup>2+</sup> can specifically cause fluorescence enhancement.

Cu<sup>I</sup>-catalyzed azide/alkyne cycloaddition (CuAAC) is commonly used for the detection of copper ions. The reaction of azide and alkyne is extremely slow, but the reaction rate can be greatly improved with the catalysis of Cu<sup>I</sup>. Moreover, the reaction takes place at room temperature, does not require an inert atmosphere, and the products are stable. These features make the CuAAC reaction a mild sensing strategy, and its main advantage is its dependence on the catalytic activity of copper. Jiang et al. introduced a quick and simple fluorescent assay based on CuAAC for detecting free Cu ions in patient urine samples without complex pretreatment [75], as shown in Figure 3A. The assay utilizes a click reaction between graphene oxide and a fluorescent dye. This reaction can be triggered promptly by Cu<sup>2+</sup>, thus allowing the detection of Cu ions with outstanding sensitivity and selectivity in under a minute. Additionally, the system can be read values with a smartphone using color scan software (Figure 3B). Similarly, Chen et al. developed a cascade signal amplification strategy to detect Cu<sup>2+</sup> [76], which is combined with a substrate consisting of gold nanorods coupled with silver nanoislands to enhance fluorescence. In addition, the Raibaut group proposed a turn-off luminescent peptide for Cu<sup>2+</sup> [77], which proved suitable for the detection of copper ions by time-resolved luminescence detection.

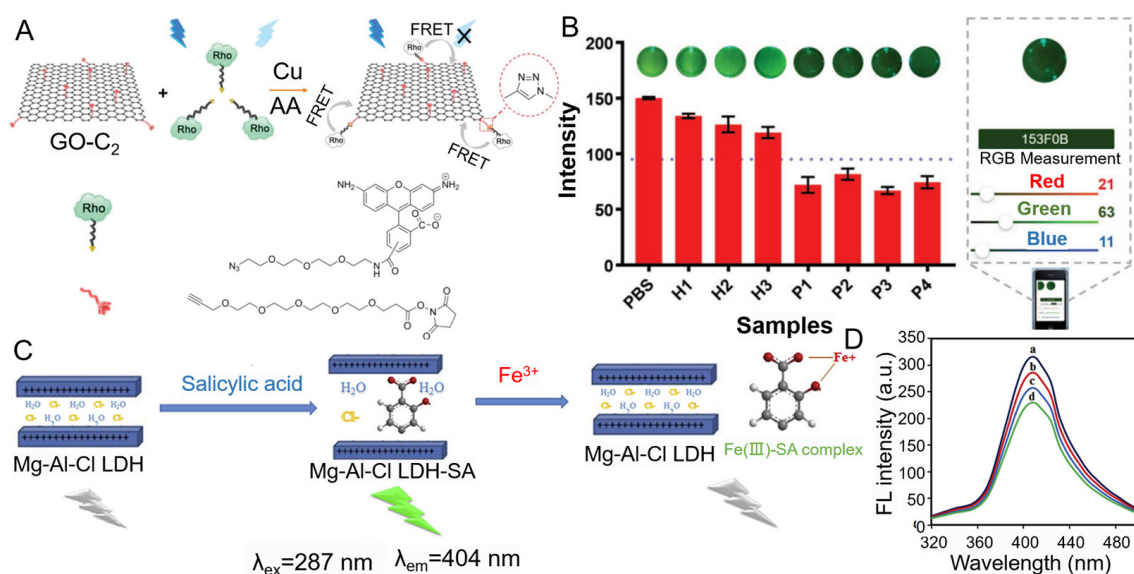


**Figure 3.** Two representative examples of essential metal ion detection in vitro: (A) Schematic illustration of the Cu<sup>2+</sup> detection system based on click chemistry and FRET between GO-C2 and Rho-N3. (B) Detection Cu in patient urine by reading the green value of the photo of the samples using the smartphone. Reproduced from [75] with permission from John Wiley and Sons, copyright 2018. (C) Schematic illustration of the Fe<sup>3+</sup> detection system based on nano-structured Mg-Al layered double hydroxide intercalated with salicylic acid (Mg-Al LDH-SA). (D) The fluorescence emission spectra of the deproteinized human serum sample before (a) and after adding a standard solution of Fe<sup>3+</sup> (b–d). Reproduced from [18] with permission from Elsevier, copyright 2019.

### 3.1.5. $\text{Ca}^{2+}$

Calcium ( $\text{Ca}^{2+}$ ) is the most abundant signal transduction messenger in cells, and calmodulin (CaM) is a widespread  $\text{Ca}^{2+}$  sensor in eukaryotic cells [78]. Carbon dots (CDs) are a class of zero-dimensional fluorescent carbon nanomaterials. Motivated by the  $\text{Ca}^{2+}$  sensing process of CaM, Lin et al. explored a new CD-based  $\text{Ca}^{2+}$  sensor by using a CaM mimetic peptide as a functional group [79]. CDs functionalized with synthetic peptides can target  $\text{Ca}^{2+}$  specifically in biologically relevant media, leading to an effective fluorescence burst. In addition, the f-CD sensor is highly biocompatible and can be used for the quantitative detection of free  $\text{Ca}^{2+}$  in serum.

Metal-organic frameworks (MOFs) are a relatively new type of chemical sensor with internal pores that can be used to interact with different analytes [80,81]. Masoomi's team first reported MOFs-based calcium-sensitive probes (TMU-5S) by introducing rhodamine B into the framework of TMU-5 [82]. As a ratiometric fluorescent sensor, this dye-sensitized MOF allows  $\text{Ca}^{2+}$  signaling in the presence of interfering cations similar to plasma ion concentrations and exhibits exceptional sensitivity and selectivity for  $\text{Ca}^{2+}$  in the blood.

### 3.1.6. $\text{Fe}^{3+}$

The iron content of human serum ranges from 14–32  $\mu\text{M}$ . Since iron is critical for hemoglobin synthesis and oxidation reactions in the body, iron deficiency and excess can lead to various diseases. Monireh's team developed Mg-Al LDH-SA nanomaterials, which are composed of Mg-Al layered double hydroxides sandwiched by salicylic acid [18], as shown in Figure 3C. The nanosensor emits at 404 nm under excitation at an excitation wavelength of 287 nm. When Mg-Al LDH-SA encounters iron ions, the iron ions and salicylic acid will form a stable complex, which leads to the decrease of its fluorescence signal. In addition, this method was successfully used to measure ferric ions in human serum samples (Figure 3D). Another promising  $\text{Fe}^{3+}$  sensor based on 2,5-dihydroxyterephthalic acid (DOBDC)- $\text{Zn}^{2+}$  MOFs (ZnMOF-74) was developed by Li et al. [83]. The DOBDC phenolic hydroxyl groups are reactive to  $\text{Fe}^{3+}$ , leading to cation conversion between  $\text{Fe}^{3+}$  and  $\text{Zn}^{2+}$ . This results in skeleton collapse, causing quenching of the active fluorescence of ZnMOF-74. This fluorescence probe successfully detected  $\text{Fe}^{3+}$  in human serum with high accuracy and recovery. Later, the Zhang group synthesized fluorescent CDs from brewer's spent grain and used them as label-free probes for  $\text{Fe}^{3+}$  detection [84]. The sensor exhibited a linear detection range of 0.3–7  $\mu\text{M}$  with an LOD of 95 nM and was successfully applied for practical  $\text{Fe}^{3+}$  determination in FBS.

## 3.2. Fluorescent Sensors for Non-Essential Metal Ions

### 3.2.1. $\text{Ag}^+$

Ag is a typical heavy metal ion, and its toxic effects on DNA replication and protein function make the detection of Ag of great interest. Particularly, the accurate detection of Ag in biospecimens is crucial through fluorescence analysis. Feng et al. proposed a facile method to synthesize hyperfluorescent N-dots, employing 2-azidazole and hydroxyl compounds as cross-linking additives (Figure 4A) [85]. The nanomaterials exhibited excellent stability against various factors and can be used as sensors for  $\text{Ag}^+$  sensing. The sensing mechanism is based on the static quenching effect between N-dots and silver ions. The resulting sensor showed good linearity in the range of concentrations from 20 nM to 6  $\mu\text{M}$  and a detection limit of 6.3 nM, and more importantly, it displayed high specificity for silver ions in human urine.

### 3.2.2. $\text{Pb}^{2+}$

Lead ions are a highly toxic type of pollutant that can contaminate soil and water, posing a threat to food safety. Their accumulation in the body is difficult to eliminate and can lead to severe nerve, hematopoietic, and renal damage, ultimately resulting in death. Nucleic acid-based sensors are frequently used for lead ion detection. Xu et al. designed a highly sensitive cascade signal amplification sensor that combines DNAzyme-

based strand displacement amplification with HCR to sense  $\text{Pb}^{2+}$  [86], while Jia's group developed a novel strategy for  $\text{Pb}^{2+}$  detection based on a fluorophore-tagged  $\text{Pb}^{2+}$ -binding aptamer [87], as shown in Figure 4B. Since the binding of the aptamer to  $\text{Pb}^{2+}$  leads to a conformational change, the original low-fluorescence “off” state becomes a high-fluorescence “on” state. The method enables quantitative detection of lead ions with a minimum detection concentration of 468 nM, maintaining high specificity for  $\text{Pb}^{2+}$  during the detection process. Furthermore, it has been successfully tested in complex biofluids (Figure 4C), making it a promising tool for  $\text{Pb}^{2+}$  detection in practical applications. Tang and colleagues designed an innovative method for the direct detection of  $\text{K}^+$  and  $\text{Pb}^{2+}$  with high selectivity and sensitivity [88], which relies on the assembly and disassembly of a chiral cyanine dye/TBA complex. Lee et al. [89] synthesized fluorescent probes by incorporating a peptide receptor with hard and soft ligands and a benzothiazolyl-cyanovinylene fluorophore, which were successfully utilized for  $\text{Pb}^{2+}$  quantification in human serum.

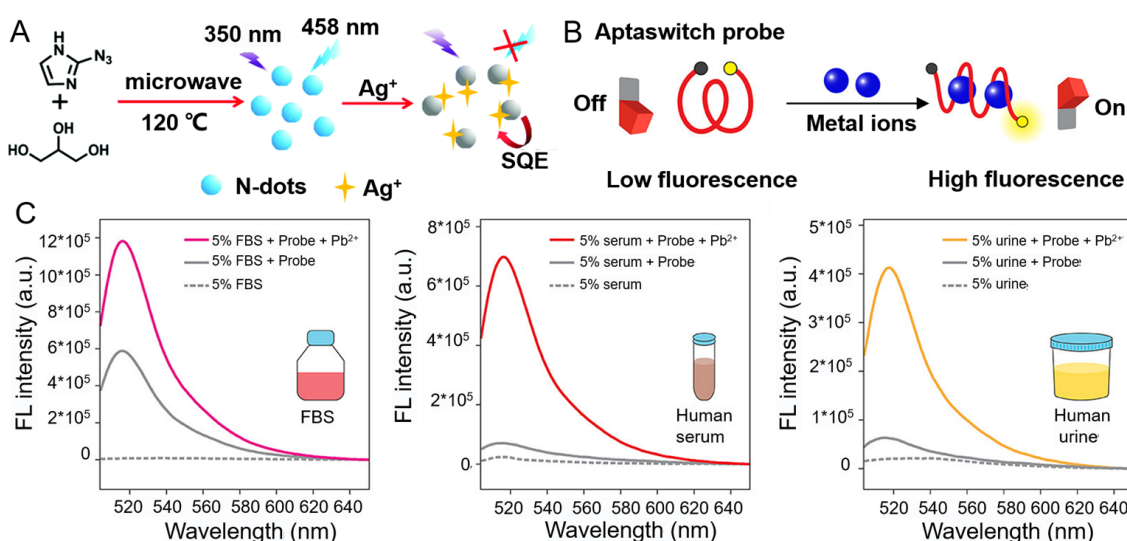


**Figure 4.** Two representative examples of non-essential metal ion detection in vitro: (A) Illustration of the synthesis process of nitrogen-rich CDs (N-dots) and the detection of  $\text{Ag}^+$ . Reproduced from [85] with permission from the Royal Society of Chemistry, copyright 2019. (B) Concept of  $\text{Pb}^{2+}$  detection using a fluorescent signal-on aptamer sequence (aptaswitch). (C) Detection of  $\text{Pb}^{2+}$  in biological fluids by the aptaswitch probe. Reproduced from [87] with permission from the American Chemical Society, copyright 2022.

### 3.2.3. $\text{Hg}^{2+}$

Mercury contamination is a global concern due to its toxic and mutagenic effects. A highly sensitive and specific label-free fluorescent sensor for mercury ions was developed by the Wang group [90]. This sensor utilized the split GQ/dsDNA assembly and Thioflavin T as a reporter and has been successfully applied to detect  $\text{Hg}^{2+}$  levels in fetal calf serum. Subsequently, they obtained dual fluorescent signals by using two fluorescent dyes and T-rich/G-rich terminal DNA sequences on proportional mercury induction [91].

Nilanjan synthesized a highly sensitive and selective probe for detecting  $\text{Hg}^{2+}$  at ppb levels in aqueous medium [92], as illustrated in Figure 5A. The probe is based on pyridine-coupled dibenzimidazole, which displayed the charge-transfer interactions and coordinated driving of the planarization of the biphenyl backbone. As a result, it exhibited a red-shifted absorbance and fluorescence peak in the presence of mercury ions. The dual mode sensing approach enables accurate and reliable detection of  $\text{Hg}^{2+}$  in the presence of albumin protein (Figure 5B). Moreover, the probe-coated paper strip could remain colorless under normal daylight but exhibit blue fluorescence under UV flashlight irradiation (Figure 5C).

This feature can be used for rapid, on-site detection of  $\text{Hg}^{2+}$ , highlighting its potential in environmental monitoring and biomedical research.

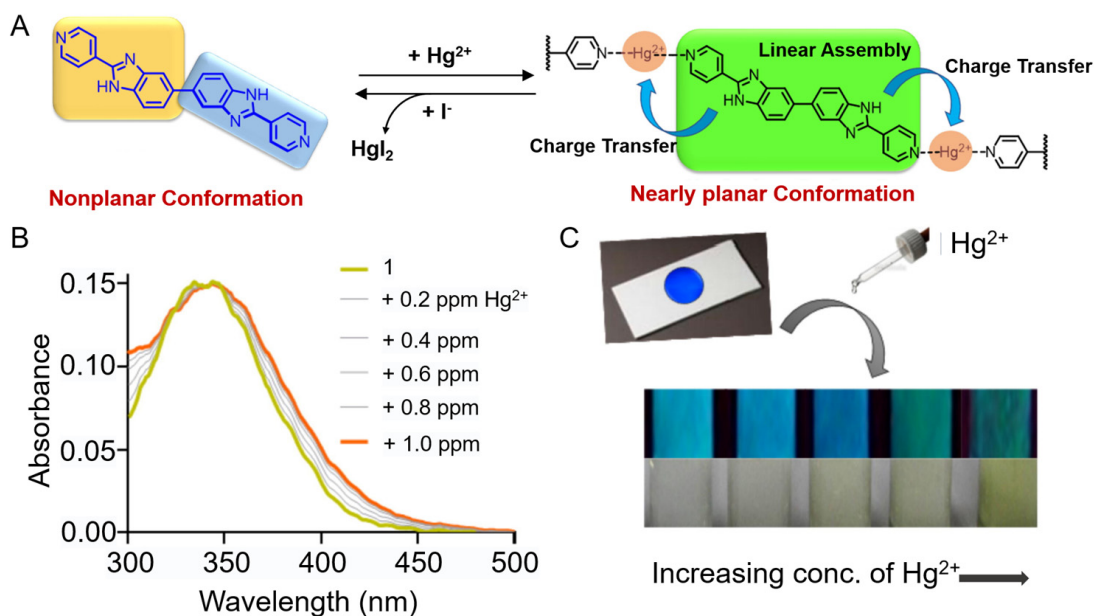


**Figure 5.** (A) Schematic diagram shows simultaneous sensing of  $\text{Hg}^{2+}$  and  $\text{I}^-$  via reversible supramolecular assembly formation. (B) Titration of 1  $20 \mu\text{M}$  with  $\text{Hg}^{2+}$  (0–1 ppm) in the presence of 0.1 mg/mL HSA at pH 7.0. (C)  $\text{Hg}^{2+}$  induced changes in the color of paper strips (0–2 ppm) under normal daylight and UV light. Reproduced from [92] with permission from Elsevier, copyright 2021.

### 3.2.4. $\text{Al}^{3+}$

Aluminum, the most abundant metallic element in the Earth's crust, has extensive applications in our daily lives. However, excessive intake of aluminum can lead to serious health problems and central nervous system dysfunction. To address this issue, Huang's team developed a highly efficient and versatile bifunctional fluorescence sensor based on benzimidazole [93], which can rapidly and accurately detect changes in pH and  $\text{Al}^{3+}$  in aqueous solutions. With a simple and effective detection mode, the sensor can detect  $\text{Al}^{3+}$  in a variety of real samples, including water, food, beverages, drugs, serum, and urine. These promising results demonstrate the sensor's potential for broad applications in the field of metal ion sensing.

### 3.2.5. $\text{Pt}^{4+}$

Platinum ion accumulation in the body can lead to toxicity, renal failure, cognitive and motor impairment, and severe neurological disorders. Considering the significant rise in Pt ion chemicals and the associated toxicity, it is crucial for the development of facile and rapid methods to monitor the presence of Pt species in physical and environmental settings. Liang and colleagues designed a highly sensitive and selective nanosensor (PEIMP) for the specific determination of  $\text{Pt}^{4+}$  in aqueous media [94]. The nanosensor is based on a novel hydrophilic polymer and shows a linear range of 0.1–10  $\mu\text{M}$  and an ultra-low detection limit of 80 nM. The sensing mechanism is based on an "on/off" switching process of photoinduced electron transfer (PET), which allows enhanced fluorescence detection of  $\text{Pt}^{4+}$ . This method has been successfully applied for the quantification of  $\text{Pt}^{4+}$  in wastewater and urine samples and shows great potential for monitoring  $\text{Pt}^{4+}$  in biological systems.

## 4. Intracellular Imaging of Metal Ions

Our understanding of the effects of metal ions on physiological processes can be deepened by detecting them in living cells. Since the 1960s, the use of fluorescent sensors for cellular and molecular imaging has proliferated due to advances in image processing

technology. This imaging technique can be used for disease identification, tracking, and treatment, as well as for the detection of several biomarkers. Fluorescence imaging can expose the structural and physiological characteristics of cells and tissues, and also measure intracellular molecules and molecular structures [39]. Recently, there have been significant improvements in the sensitivity and selectivity of metal ion detection by advances in bioimaging.

#### 4.1. Fluorescent Sensors for Essential Metal Ions

##### 4.1.1. Na<sup>+</sup>

Schiff base ligands possess excellent photochemical properties and can be used to create fluorescent probes, but the use of sodium (I) complexes based on Schiff base ligands is rare [95]. Tamilselvi et al. recently designed a sodium ion sensor based on a pyridoxal-bearing triazole ring Schiff base [96], which exhibits strong blue-green emission in the solid state and emits a yellow light when Na<sup>+</sup> is present. They further studied the proportional fluorescence response of this probe with sodium ions in the U87 cell line, indicating its potential application in cell biology protocols.

Potassium and sodium play crucial roles in various biological processes, but their synergies also have important implications for various biological processes. Yang et al. designed the first cell-surface fluorescent probe that can simultaneously detect Na<sup>+</sup> and K<sup>+</sup> in the microenvironment of cells [97]. The probe utilizes a Y-shaped DNA sensor composed of three distinct DNA sequences: a Na<sup>+</sup>-specific enzyme strand hybridized with the substrate strand and a GQ strand that binds to K<sup>+</sup>. The use of this probe to detect Na<sup>+</sup>/K<sup>+</sup> concurrently provides a more comprehensive understanding of the dynamic changes of the targets than single-ion assays. The design and use of this probe have great significance in further understanding Na<sup>+</sup> and K<sup>+</sup>-related cellular events and biological processes.

##### 4.1.2. K<sup>+</sup>

For imaging intracellular K<sup>+</sup>, it is vital to develop a molecular recognition element that can achieve high affinity and selectivity to K<sup>+</sup>. Tian et al. presented the first polymer-based ratiometric fluorescent K<sup>+</sup> indicator (PK1), which was modified with a water-soluble polymer skeleton to enable high-throughput monitoring of K<sup>+</sup> fluctuations in living cells [98]. Subsequently, they further enhanced the detection of potassium ions in cells by incorporating a small-molecule K<sup>+</sup> fluorescent probe into a hydrophilic F127 block and then binding it to cationic liposomes to create modified nanoparticles with enhanced cellular affinity [99]. A pioneering chemosensor for the accurate intracellular ratiometric imaging of potassium using a dual fluorophore strategy was introduced by Chang et al. [100]. Furthermore, Chen et al. innovated a remotely operated “lock-unlock” nanosystem [101]. This nanosystem utilizes a dual-stranded aptamer precursor (DSAP) as the recognition molecule and a SiO<sub>2</sub>-based gold nanoshell (AuNS) as the nanocarrier, with NIR light as the stimulus for remote application, as shown in Figure 6A. AuNS generates an increased local temperature upon receiving NIR light, which induces the dehybridization of DSAP, activates the binding capability of the aptamer, and enables the monitoring of intracellular K<sup>+</sup> via changes in the fluorescence signal (Figure 6B). This DSAP-AuNS nanosystem provides a new means to visualize endogenous K<sup>+</sup> in living cells.

##### 4.1.3. Ca<sup>2+</sup>

Fluorescent sensing and imaging have become useful tools to investigate the signaling pathways of calcium ions, which act as a widespread secondary messenger and play an essential role in neurodegenerative diseases. Modified with a specific Ca<sup>2+</sup> chelator ligand with two formaldehyde groups, a copper nanocluster ratiometric fluorescent probe was developed for real-time sensing and imaging of Ca<sup>2+</sup> in neurons [102]. In another example, an inner-filter-mediated luminescence probe was developed by using biomass quantum dots as a fluorescent reporter. This probe was initially quenched by a Ca<sup>2+</sup> chelator alizarin red S yet turned on after binding to intracellular Ca<sup>2+</sup>. Despite fluorescent nanoclusters

and quantum dots, green fluorescent protein could also be combined with the specific chelator for  $\text{Ca}^{2+}$  imaging [103]. Mitochondrial  $\text{Ca}^{2+}$  concentration in living cells is also of great importance. Mt-fura-2, the first ratiometric chemical  $\text{Ca}^{2+}$  probe for mitochondria, was developed by coupling two triphenylphosphonium cations to the molecular backbone of the ratiometric  $\text{Ca}^{2+}$  indicator fura-2 [104]. Mt-fura-2 binds calcium ions *in vitro* with a dissociation constant of  $\approx 1.5 \mu\text{M}$  and exhibits correct mitochondrial localization and precise measurement of matrix  $[\text{Ca}^{2+}]$  changes in cells.

$\text{Ca}^{2+}$ -specific DNAzyme, which was first reported in 2017 [105], was used to construct a SERS-fluorescence dual-mode probe for  $\text{Ca}^{2+}$  imaging in living cells in 2021 by Li and co-workers [106]. The  $\text{Ca}^{2+}$ -responsive nanoprobe was constructed by modifying DNAzyme and a Cy5-labelled substrate strand on gold nanostars. When the two chains hybridize, the fluorescence of Cy5 is quenched, which enhances the SERS signal concurrently. The substrate chains could be cleaved and freed from the surface of the gold nanopillar by the catalytic induction of  $\text{Ca}^{2+}$ , which leads to the weakening of the SERS signal, as well as the fluorescence signal recovery. The nanosensor has been successfully used in HeLa cells under the treatment of T-2 toxin, which increased the intracellular free  $\text{Ca}^{2+}$  concentration and caused cell apoptosis. Moreover, the calmodulin domain and its cognate M13 peptide have also been widely used in biological research. Rhodamines are highly bright and photostable fluorophores, and one of their key properties is that they exist in a balance between the non-fluorescent, spirocyclic form and the fluorescent, amphoteric form. The remarkable ability of HaloTag7 to affect rhodamine spirocyclization was used to develop biosensors in which the analyte affects the conformation of HaloTag7 and thus the balance of spirocyclization. The Johnson group developed a ratiometric biosensor based on spirocyclization in an environmentally sensitive discolored fluorophore that reversibly switches between the green and red fluorescent forms, successfully imaging calcium ions in living cells [107], as shown in Figure 6C. This biosensor combines a HaloTag7 and a  $\text{Ca}^{2+}$ -sensing structural domain (rHCaMP) to enable reversible switching between green and red fluorescent forms through intramolecular spirocyclization by using a color-shifted fluorophore. The biosensor provides precise ratiometric measurements of  $\text{Ca}^{2+}$  both *in vitro* and intracellularly (Figure 6D). Furthermore, by coupling the CSFs to various protein ligands, the biosensor achieves exceptional sensitivity, with some probes demonstrating up to 2400-fold changes in fluorescence ratios upon binding to the target. The Campbell group developed a NIR genetically encoded indicator using a biliverdin-binding fluorescent protein for multi-color imaging [108]. BAPTA could form a chemigenetic indicator due to the interaction between the BAPTA moiety and the GFP chromophore, which provided creative guidance in the design of chemigenetic indicators. In addition to fluorescent intensity-based readout, the Goedhart group also proposed a turquoise fluorescence lifetime-based biosensor for quantitative imaging of intracellular  $\text{Ca}^{2+}$  with a low sensitivity for pH, which was a teaser for traditional intensity-based indicators [109].

#### 4.1.4. $\text{Zn}^{2+}$

Accurately monitoring the zinc profile and levels in living cells is crucial for various biological studies. Among various developed methods, DNAzyme-based sensors are at the forefront of zinc ion imaging studies. However, their application in cells is limited due to the difficulty in maintaining the activity of RNA-cleaving DNAzymes during delivery and poor biological imaging performance [110,111]. To address this issue, Zhang et al. constructed a TP imaging probe based on an RNA-cleaving DNAzyme by modifying the  $\text{Zn}^{2+}$ -specific DNAzyme with TP fluorophores and utilized gold nanoparticles (AuNPs) for efficient intracellular delivery [112]. This NIR light-excited probe exhibits exceptional imaging capabilities for  $\text{Zn}^{2+}$  in viable cells and tissues, with remarkable in-depth penetration of tissues reaching depths of 160  $\mu\text{m}$ . The Lu group developed a new fluorescent imaging technique that allows for ratiometric imaging of  $\text{Mg}^{2+}$  and  $\text{Zn}^{2+}$  in living cells [113], using DNAzyme-mediated, genetically encoded fluorescent proteins. The merit of this approach is that  $\text{Mg}^{2+}$ -dependent multi-round cleavage of the target mRNA by DNAzyme activity

allows for a correlation between the expression level of fluorescent proteins and the concentration of the target metal ion. This sensor can utilize a variety of metal-specific DNAzyme, greatly expanding the range of metal ions that can be imaged with genetically encoded proteins. Additionally, Luo et al. developed a DNAzyme-based normalized strategy for direct quantification of endogenous zinc in living cells [114]. Recently, Li's team described the first example of DNAzyme-based sensors for subcellular metal-ion imaging [115], which combines a photoactivatable DNAzyme sensor probe with upconversion nanotechnology and organelle-localized strategies. Except for DNAzyme-based sensors [116], Schiff base based chemosensors [117,118], peptide-based sensors [119] and single red fluorescent protein-based sensors [120] also offer a variety of options for researchers when studying the distribution and concentration of zinc ions in living cells.

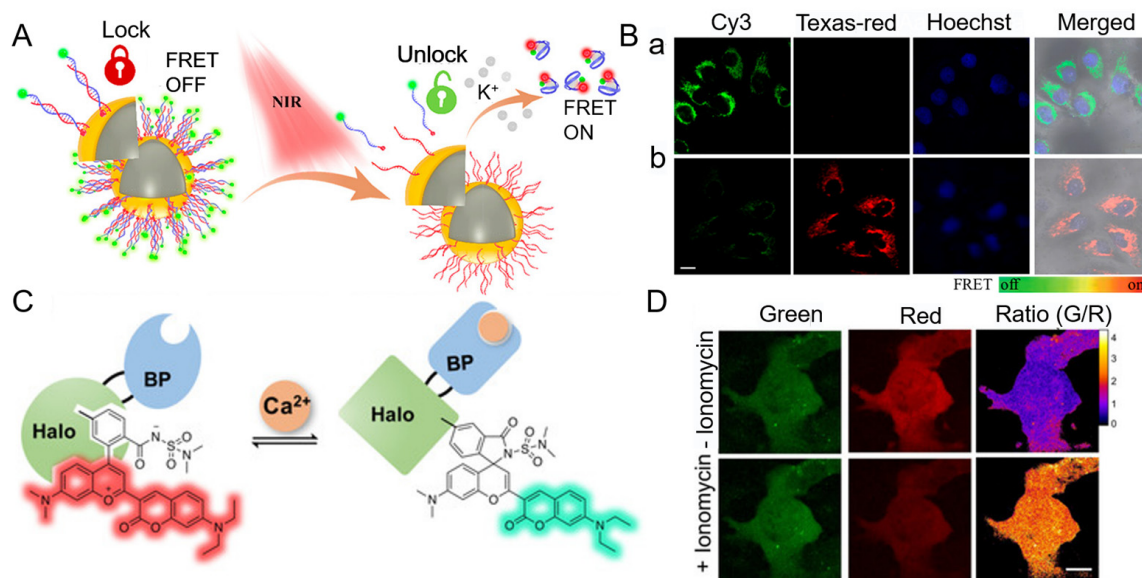


**Figure 6.** Two representative examples of essential metal ion detection in living cells: (A) Schematic illustration of the in situ imaging of  $K^+$  via the DSAP-AuNS nanosystem. (B) Confocal microscopy images of HeLa cells treated with (a) DSAP-AuNS and (b) DSAP-AuNS + NIR. Reproduced from [101] with permission from the American Chemical Society, copyright 2020. (C) Cartoon of the CSF-based semisynthetic  $Ca^{2+}$  biosensor.  $Ca^{2+}$  binding induces a conformational change, thereby shifting the equilibrium between red and green fluorescent forms. (D) Live cell  $Ca^{2+}$  imaging with rHCAMP-8. U2OS cells expressing rHCAMP 8 and treated with ionomycin (1  $\mu$ M) prior to imaging. Reproduced from [107] with permission from John Wiley and Sons, copyright 2020.

#### 4.1.5. $Mg^{2+}$

As the second largest intracellular cation after potassium, the magnesium ion is essential for various biological processes and physiological functions. However, traditional fluorescent chemosensors for the detection of magnesium ions currently face the limitations of low selectivity and poor fluorescence signal enhancement. Yuki et al. overcame this limitation by synthesizing the first highly selective and NIR fluorescent probes for the detection of  $Mg^{2+}$  [121], as shown in Figure 7A. These probes consisted of charged  $\beta$ -diketones as specific bound spots for  $Mg^{2+}$  and Si-rhodamine remnants as NIR fluorophores. They are primarily located in the cytoplasm and are localized partially in the lysosomes and mitochondria of cultured rat hippocampal neurons (Figure 7B). Moreover, the Aharon group reported the first example of aqueous CDs with high selectivity for intracellular  $Mg^{2+}$  detection [122]. Furthermore, Ashok's team successfully synthesized novel chromone-based chemosensors (La and Lb) that are highly sensitive to  $Mg^{2+}$  [123], with La also showing potential for  $Mn^{2+}$  detection through absorption studies. On the other hand, Lb was found to sense  $Cu^{2+}$  through absorption studies and also showed sensitivity

to  $Mg^{2+}$  via emission studies. These ligands were successfully used for  $Mg^{2+}$  imaging in HeLa cancer cells.

#### 4.1.6. $Cu^{2+}$

The development of copper ion sensors in recent years has still primarily relied on the design of organic fluorescent probes [124,125] and nanomaterials [126]. In the previous section, it was mentioned that the Cu(I)-catalyzed click reaction has a high selectivity for  $Cu^{2+}$ , making it ideal for complex intracellular environments. Bu et al. developed an innovative “OFF–ON” fluorescent biosensor by combining the Cu(I)-catalyzed click reaction with a 3D DNA walker based on spherical nucleic acid [127]. In the initial “OFF” state, the fluorophore (Cy3) on the hairpin is close to the surface of AuNPs, resulting in quenched fluorescence. Cu is rapidly produced in situ from  $Cu^{2+}$  in the presence of ascorbic acid, triggering the click reaction-based 3D DNA walker. The activated swing arm hybridizes with the neighboring Cy3-hairpin and drives the 3D DNA walker by endonuclease to produce several Cy3-labeled DNA fragments away from the AuNP surface, resulting in a restored fluorescence response (transitioning to the “ON” state). The utilization of this assay provides a means for transducing signals and assessing intracellular  $Cu^{2+}$  at picomolar concentrations.

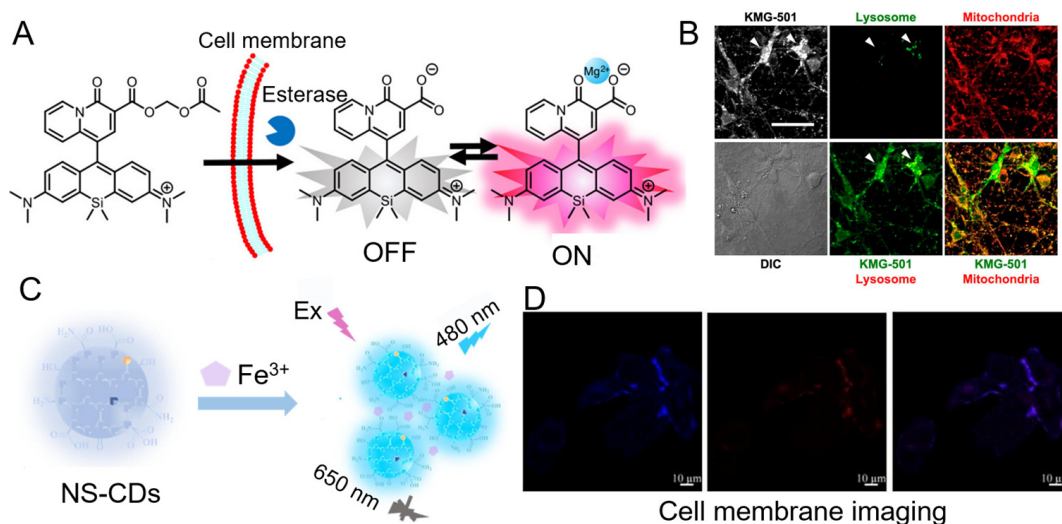


**Figure 7.** Two representative examples of essential metal ion detection in living cells: (A) Schematic illustration of the intracellular imaging of  $Mg^{2+}$  via KMG-500 series probes. (B) Intracellular localization of KMG-501 in the whole cell body of cultured hippocampal neurons. Reproduced from [121] with permission from the American Chemical Society, copyright 2020. (C) Schematic illustration of NS-CDs for the ratiometric response to  $Fe^{3+}$  and cell membrane imaging. (D) NS-CDs for targeted cell membrane imaging. Reproduced from [128] with permission from Elsevier, copyright 2021.

#### 4.1.7. $Fe^{2+}/Fe^{3+}$

CDs have garnered significant attention in metal ion detection in living cells. To this end, double-emission CDs (NS-CDs) with varying dimensions of nitrogen/sulfur doping were synthesized by solubilizing sodium alginate (SA) and glutathione (GSH) in formamide for heat treatment [128], as shown in Figure 7C. Since  $Fe^{3+}$  induces the aggregation of NS-CDs, which enhances the fluorescence signal. Therefore, this nanosensor enables ratiometric measurements of iron ions and exhibits remarkable detectability and sensitivity, with detection limits as low as 0.56  $\mu M$ . Moreover, NS-CDs display unparalleled capability for localized, specific cell membrane imaging (Figure 7D). Similarly, the Guo group proposed the synthesis of N-CDs utilizing fresh tea leaves and urea [129], while Zhang’s team fabricated deferoxamine-inspired CDs using L-aspartic acid (Asp) and 2,5-diaminobenzenesulfonic acid (DABSA) as reactants in a single-boiler hydrother-

mal synthesis [130]. Both N-CDs and deferoxamine-inspired CDs were applied for cell imaging of  $\text{Fe}^{3+}$  and exhibited promising results. Hou et al. developed an innovative “turn-on” fluorescent probe using rhodamine 6G derivatives and spirolactam ring-opening reactions [131]. This probe is highly effective in detecting  $\text{Fe}^{3+}$  for fluorescence imaging in living cells. In addition, Wang et al. designed dual-targeting fluorescent probes that combine galactose and imidazole to detect  $\text{Fe}^{3+}$  in the hepatic lysosome [132], enabling both hepatic and lysosomal targeting. Although indole-based fluorescent sensors for  $\text{Fe}^{3+}$  detection are rare, Nantanit reported three new sensors with fluorescence responses to  $\text{Fe}^{2+}$  and  $\text{Fe}^{3+}$  sensing in aqueous buffer systems [133]. One of these isomers is an excellent candidate for tracking  $\text{Fe}^{3+}$  in biological systems.

#### 4.2. Fluorescent Sensors for Non-Essential Metal Ions

##### 4.2.1. $\text{Li}^+$

The lithium-based complex is a widely used and effective drug for the treatment of bipolar disorder (BD) for more than 70 years. The distribution of lithium ions in the patient’s cells is crucial to optimize the therapeutic effect. However, imaging lithium selectively in the biomedically relevant concentration range (0.5–2.0 mM) in living cells remains a major challenge. A major breakthrough was recently reported by Lu’s team, which developed a lithium-specific DNAzyme with a selectivity exceeding 100-fold that of other biologically relevant metal ions [134], as shown in Figure 8A. This novel sensor allows for the visualization of lithium in HeLa cells, neurons from BD patients, healthy controls (Figure 8B) and human neuronal progenitor cells (Figure 8C) for comparison, making it a promising tool for investigating the therapeutic effects of lithium.

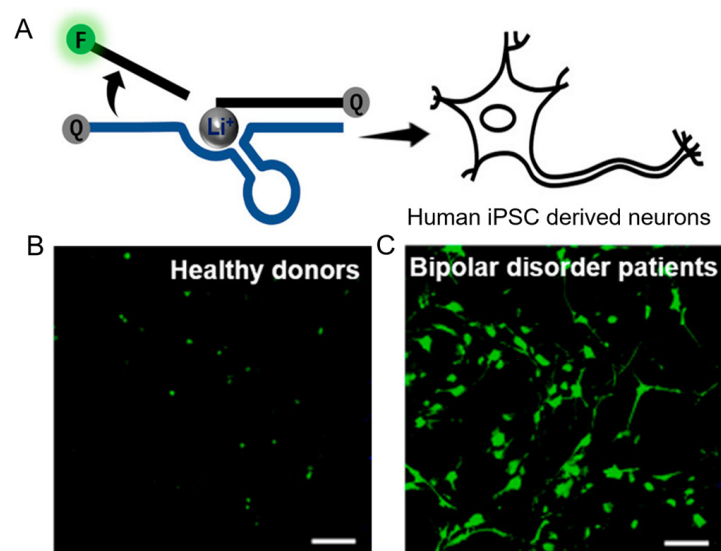


**Figure 8.** (A) Design of the  $\text{Li}^+$  DNAzyme catalytic beacon. Intracellular  $\text{Li}^+$  imaging in neural progenitor cells of (B) healthy donors; and (C) bipolar disorder patients. Reproduced from [134] with permission from the American Chemical Society, copyright 2021.

##### 4.2.2. $\text{Ag}^+$

Dong et al. developed a label-free N-CDs system for the detection of silver ions and GSH through intrinsic ratiometric fluorescence [135]. The N-CDs emit a single long-wavelength light at 618 nm when excited at 478 nm. When silver ions are present, this nanosensor shows a rising peak at 532 nm and a decrease in emission at 618 nm, enabling the detection of silver ions in the range of 0–140  $\mu\text{M}$ . Yu et al. presented a groundbreaking approach to visualize  $\text{Ag}^+$  in living bacterial cells by utilizing a genetically encoded biosensor (Figure 9B) [136]. The sensor incorporates a cytosine- $\text{Ag}^+$ -cytosine metal base pair into a fluorogenic RNA aptamer, known as Broccoli, which folds and emits a fluorescent signal

upon binding to  $\text{Ag}^+$  (Figure 9A). This unique RNA sensor can be further adapted for cellular imaging of other metal ions by implementing a similar design principle based on specific metal base pairs.

The Guo group synthesized a novel ratiometric chemosensor called CHa based on the hydrolysis of hydrazone derivatives of coumarin fluorescent moieties induced by  $\text{Ag}^+$  [137]. When CHa encounters silver ions, it undergoes hydrolysis, resulting in the release of a 3-formyl-substituted coumarin derivative that acquires blue emission at short wavelengths from yellow emission. Additionally, a phenanthro [9,10-d] imidazole-based fluorescent probe with AIE activity was designed by Bu et al. [138], for simultaneous sensing of  $\text{Ag}^+$  and  $\text{SCN}^-$ . In another example, a sustainably modifiable 1,2-alternating thiacalix[4]arene was synthesized by Yu et al. [139], which displayed a highly sensitive ratio recognition for  $\text{Ag}^+$ .

#### 4.2.3. $\text{Ni}^{2+}$

Nickel ions play a vital role as a cofactor for a variety of microbial enzymes, supporting essential cellular functions necessary for prokaryotic survival. A FRET-based genetically encoded biosensor was developed by Neha [140], taking enhanced cyan fluorescent protein and Venus (a variant of yellow fluorescent protein) respectively into account as donor and acceptor fluorescent molecules. Such sensors permit concentration-dependent monitoring of nickel ion fluxes within viable cells with a high spatial and temporal resolution to provide in-depth insight into the distribution of nickel ions physiologically at the cellular and subcellular levels.

Reports on fluorescent probes for nickel ions are relatively scarce, and there is still a need to develop simple and effective detection methods. Wang et al. constructed a molecular probe FA-Ni to achieve highly selective and ultrasensitive rapid detection of  $\text{Ni}^{2+}$ , avoiding the interference of other ions [141]. Nickel ions were converted to elemental nickel under the reducing conditions of  $\text{NaBH}_4$ , and then triphenylphosphine was used as a ligand to detach allyl from the probe FA-Ni, thereby generating a fluorescent signal. They also successfully applied the probe FA-Ni for in situ imaging of nickel ions in living cells. Additionally, Shahzad's team reported AIE active sensors for the detection of  $\text{Ni}^{2+}$  in live cells and acid/base sensing [142]. Gu et al. developed a new chemosensor based on a pyrazolopyrimidine core that can simultaneously detect  $\text{Cu}^{2+}$  and  $\text{Ni}^{2+}$ , which has good imaging properties for both  $\text{Cu}^{2+}$  and  $\text{Ni}^{2+}$  in living cells [143].

#### 4.2.4. $\text{Pb}^{2+}$

The interaction between metals and biomolecules can be found throughout nature and provides a wealth of resources and principles of design in the search for novel, recognizable ligands. Peptides are promising candidates for designing metal-binding ligands due to their rich coordination chemistry, high stability, and availability of optional building blocks. Additionally, their high biocompatibility makes them well-suited for detecting  $\text{Pb}^{2+}$  in biological systems. The Zhao group designed a biomimetic peptide-based fluorescent sensor GSSH-2TPE inspired by the structure of glutathione [144], as shown in Figure 9C. Mechanistic studies confirmed that there is a delicate balancing between the chelating groups and the molecular configuration responsible for the highly selective complexation of  $\text{Pb}^{2+}$  by the sensor. Additionally, the ion-induced supramolecular assembly generates a bright fluorescence signal. Featuring good biocompatibility and the lowest possible disturbance to both endogenous biothiols and background fluorescence, the sensor allows precise imaging of  $\text{Pb}^{2+}$  in vivo (Figure 9D). Similarly, Mehta et al. designed a proportional fluorescent peptide-based sensor by coupling the peptide receptor of Pb(II) with an excimer-forming benzothiazolylcyanovinylene fluorophore [145].

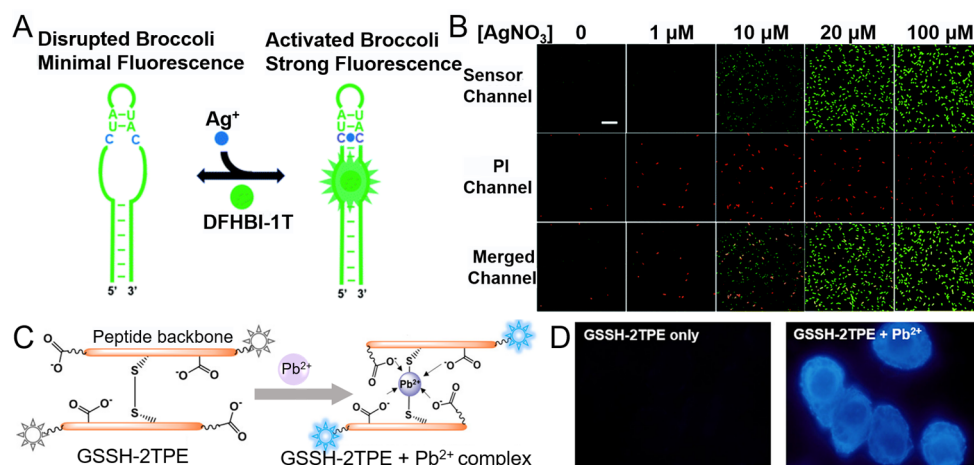


**Figure 9.** Two representative examples of non-essential metal ion detection in living cells: (A) Schematic illustration of modified Broccoli. The green region indicates sequences from the original Broccoli and the C–C mismatch is highlighted in blue. (B) Confocal fluorescence imaging of the sensor-expressing BL21 (DE3) \* cells. Reproduced from [136] with permission from the Royal Society of Chemistry, copyright 2019. (C) Possible process for the formation of the coordination complex and supramolecular assembling of fluorescent nanoaggregates from GSSH-2TPE and Pb<sup>2+</sup>. (D) Fluorescence microscopic images of living HeLa cells with GSSH-2TPE, with and without the addition of Pb<sup>2+</sup>. Reproduced from [144] with permission from the American Chemical Society, copyright 2019.

#### 4.2.5. Pd<sup>2+</sup>

Palladium is a scarce internal transition metal that is widely employed as an extremely potent catalyst in various areas. However, it should be noted that Pd species can disrupt many biological processes and pose significant health hazards. Of particular concern is Pd<sup>2+</sup>, which is the most abundant oxidation state in alive cells, thus the potential for developing validated Pd<sup>2+</sup> detection and imaging approaches are vital for environmental safety and the health of humans. Wen et al. developed a naphthofluorescein-based NIR fluorescent probe called M-PD [146], which boasts exceptional sensing properties for the detection of Pd<sup>2+</sup>. The lower limit of detection for this sensor was found to be 10.8 nM, a value significantly below the drug in threshold values (5–10 ppm). Additionally, M-PD has been successfully utilized for the near-infrared fluorescence imaging of Pd<sup>2+</sup> in living cells. A chemosensor, DCF-MPYM-Pd, featuring a wide Stokes shift and an ability for lysosomal targeting was synthesized by Wang et al. [147]. It was shown that this sensor can accurately sense palladium (II) in living cells and can specifically accumulate in lysosomes. To avoid the problem of the multi-step synthesis of a probe, Mareeswaran's group found a simple and well-known organic molecule, coumarin-460 (C460), that can selectively sense palladium ions in aqueous media [148]. They went on to validate the binding and sensing properties of C460 for Pd<sup>2+</sup> by absorption and fluorescence spectroscopy techniques, thus demonstrating that the C460 molecule can be used as an “off” probe for Pd<sup>2+</sup> for real-time detection and biological applications.

While most researchers have designed probes to detect only one form of palladium, the ability to discriminate between Pd (0) and Pd (II) has been rarely reported. In this regard, Zhang et al. designed Umb-Pd2, a corymbone-derived sensor that can be used as a tiny, robust, reliable, and detective sensor for the detection of Pd (II) [149], as shown in Figure 10A. In both the stand-alone and co-existing systems, it is distinguished from typical research by its unique selectivity for Pd (II) and Pd (0), which is commonly referred to as Pd (0)-selective. This differentiation capability was further used in the case of living cell imaging (Figure 10B).

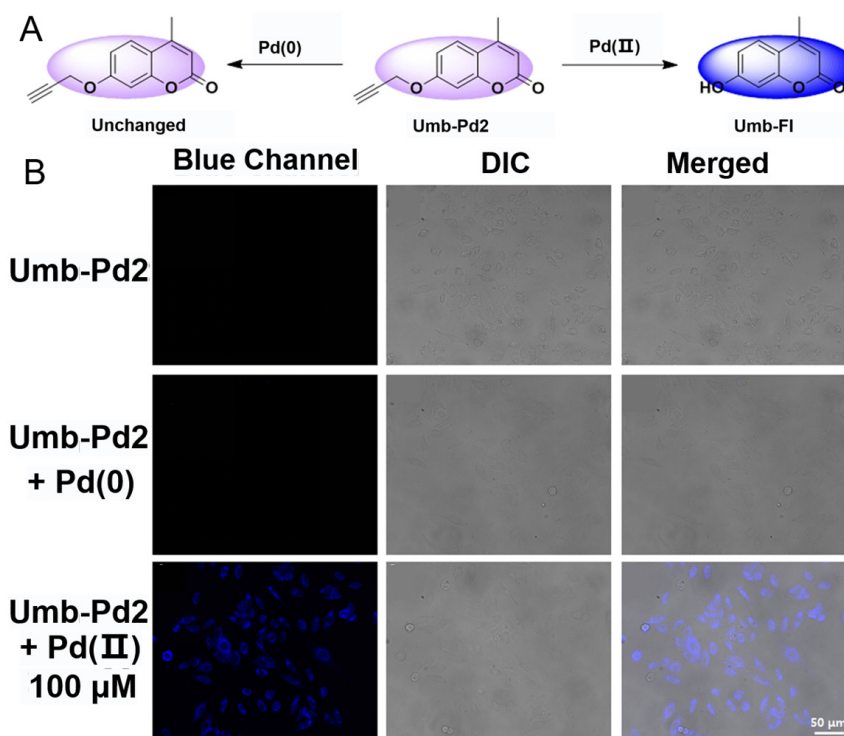


**Figure 10.** (A) Schematic illustration of the selective detection for Pd (II) by Umb-Pd2. (B) The confocal images of HeLa cells incubated with Umb-Pd2 in different conditions. Reproduced from [149] with permission from Elsevier, copyright 2019.

#### 4.2.6. Hg<sup>2+</sup>

Sarah et al. developed highly NIR fluorescent graphene quantum dots (GQDs) by pyrolyzing biomass-derived CBDA-2 in basic conditions [150]. When treated with mercury ions, the fluorescence of GQDs was quenched. Exploiting the intramolecular charge transfer (ICT) mechanism, Duan's team introduced a new phenothiazine-based sensor [151], PHE-Ad, for monitoring Hg<sup>2+</sup>. With its excellent fluorescent signaling behavior and low cytotoxicity, PHE-Ad proved to be successful in detecting and imaging Hg<sup>2+</sup> in living cells. Furthermore, the same team reported another two novel PET fluorescent probes, CH3-R6G and CN-R6G, rationally synthesized by partial doping of rhodamine 6G fluorophore with a triazolyl benzaldehyde moiety and applied with great success for Hg<sup>2+</sup> imaging in breast cancer cells [152]. Ding et al. reported the synthesis of ethyl 2,5-diphenyl-2H-1,2,3-triazole-4-carboxylate [153], which was then introduced into rhodamine B to produce a novel derivative, REDTC. This probe exhibited remarkable selectivity for Hg<sup>2+</sup> through a chromogenic reaction, without interference from other metal ions. Lastly, two novel NIR monosulfide probes, MTSQ-1 and MTSQ-2, were designed and used for Hg<sup>2+</sup> imaging based on a mercury deuteration strategy [154]. Particularly, the MTSQ-2 was packaged in a  $\beta$ -CD and showed excellent performance for imaging Hg<sup>2+</sup> in HeLa cells as well as a high signal-to-background ratio.

#### 4.2.7. Cd<sup>2+</sup>

Cadmium ions, one of the most dangerous heavy metals, can affect various cellular physiological effects. Toxic cadmium ions may lead to acute or chronic toxicity, causing cancer and other diseases. The development of highly sensitive and selective methods for the detection of cadmium ions in cells is still challenging. Lin et al. developed a highly selective probe, (E)-4-(4-([2,2':6',2''-terpyridin]-4'-yl)styryl)-1 octadecylpyridin-1-ium bromide (ZC-F8) [155]. The fluorescence spectra of ZC-F8 showed an excellent response to Cd<sup>2+</sup> through both an intramolecular charge transfer effect and an AIE effect. Moreover, the results of cell imaging experiments showed that the probe has ideal membrane permeability

and a labeled property for  $\text{Cd}^{2+}$ , indicating its promising application in the detection and tracking of metal ions in living cells. In addition, Liao's team successfully synthesized a new peptide-based probe (DSC) with good water solubility and biocompatibility, showing a fluorescent "turn-on" response to  $\text{Cd}^{2+}$  based on the PET principle [156]. Fluorescence imaging experiments showed that DSC can selectively monitor  $\text{Cd}^{2+}$  in living cells.

#### 4.2.8. $\text{Au}^{3+}$

Gold has a broad range of uses in chemistry, catalysis, and medicine. However, the binding of  $\text{Au}^{3+}$  with certain DNA and enzymes poses severe health risks, causing damage to organs. Guo et al. synthesized carbon dots by a simple solvothermal method using the acetic acid-treated peel of red dragon fruits, called ACDs [157]. With their high  $\text{sp}^2$ -hybrid carbon and carboxyl group contents, ACDs can efficiently convert  $\text{Au}^{3+}$  to  $\text{Au}^0$  and stabilize the resulting AuNPs. Electron transfer from ACD to  $\text{Au}^{3+}$  and the inner filtering effect from ACD to AuNPs synergistically quenched the fluorescence within 30 s. In addition, ACDs possessed promising photo-stability, low cytotoxicity, and favorable biological compatibility, enabling their successful application in intracellular  $\text{Au}^{3+}$  sensing and imaging.

#### 4.2.9. $\text{Al}^{3+}$

The Nikhil group synthesized a new compound, (E)-2-(benzamido)-N'-((2-hydroxynaphthalen-1-yl) methylene) benzohydrazide (BBHAN) [158], which belongs to the Schiff base derivative family and contains a hydrazine-bridged anthranilic acid-naphthalene conjugate. BBHAN is a highly sensitive  $\text{Al}^{3+}$  detection probe with a limit of detection of  $1.68 \times 10^{-9}$  M. Its detection mechanism is based on the chelation-enhanced fluorescence phenomenon, as demonstrated by time-resolved fluorescence measurements. Moreover, BBHAN is capable of detecting  $\text{Al}^{3+}$  in MDA-MB-468 cells. Later, Jessica et al. designed and synthesized a new series of Schiff base chemosensors to sense  $\text{Al}^{3+}$  [159]. The molecular solubility and compatibility of the amino acid Schiff base (A) in the presence and absence of  $\text{Al}^{3+}$  were well demonstrated. Furthermore, in human epithelial cells Hs27, the fluorescent bioimaging applications were demonstrated. In the same way, Wang et al. designed an innovative nanoprobe by co-self-assembling an amphiphilic polymer containing a Schiff-base fluorescent unit [160]. This novel nanoprobe not only provides high sensitivity for  $\text{Al}^{3+}$  imaging but also has the potential to be applicable to other ions or biomolecules by adjusting the fluorescent unit incorporated into the amphiphilic polymer.

### 5. In Vivo Imaging of Metal Ions

The imaging of living animal models offers the capacity to detect changes in signaling molecules, ions, and other biological components throughout different life stages and in the presence of disease. The information obtained from this imaging technique can be applied to discover novel biological insights or to identify markers of disease progression, thereby facilitating the development and translation of effective therapeutics. In particular, the importance of metal ions in organismal regulation, especially in terms of enzyme activation/deactivation and catalysis, and the close association with disease onset and progression make in vivo metal ion imaging a key priority for fluorescent sensor development.

#### 5.1. Fluorescent Sensors for Essential Metal Ions

##### 5.1.1. $\text{K}^+$

Potassium ions, which fluctuate in concentration, exist inside and outside cells, and can be associated with abnormal physiological functions, including nervous system disorders and cardiac dysfunction [161]. Nonetheless, probes for potassium ions perform poorly in real-time monitoring in live animal models and there is still a need to develop more sensitive probes for deep tissue monitoring. Ning et al. designed a potassium ion probe, NK2 [162], which combines colorimetric, fluorescence, and photoacoustic methods for three-channel sensing, utilizing benzylguane-6-string ether as the recognition element.

The probe extended the depotential range of  $K^+$  from 5 mM to 200 mM. In the exploration of animal models, the probe was further imaged with photoacoustic properties that allowed changes in potassium ion concentration to be monitored in the mouse ear under a photoacoustic microscope.

On the basis of NIR for deep tissue detection in live animals, a mesoporous silica nanocomposite was reported by Liu et al. [163]. The material encapsulated upconversion nanoparticles (UNCPs) and potassium ion indicators and was encapsulated within a potassium ion-specific filter membrane, which is used to monitor changes in the concentration of potassium ions in the mouse brain. The presence of the filter membrane effectively shielded the assay from other metal ions and serves to enrich the signal. This “shielded nanoparticle” is expected to be an effective method for monitoring metal ions in the brain, and in combination with endoscopic and photometric methods, could be applied to real-time potassium ion imaging. Relying on shielded nanometers, Liu et al. [164] continued to work on the development of a potassium ion sensor containing mesoporous silica nanoparticles with an embedded optical potassium indicator, as shown in Figure 11A. The nanosensor enables the spatial mapping of potassium ion release in the hippocampus of freely moving mice for precise imaging of epileptic foci in the brain (Figure 11B), also allowing for targeted drug release as needed.

#### 5.1.2. $Ca^{2+}$

Genetically encoded calcium indicators (GECIs) of the nervous system are broadly explored for calcium imaging, and the GFP-based GCaMP series of GECIs has undergone iterative updates over nearly 20 years [165]. In 2019, on the basis of GCaMP6, Dana et al. optimized jGCaMP7 by utilizing structure-guided mutagenesis and neuron-based screening [166]. This calcium sensor optimized parameters including signal-to-noise ratio and speed for in vivo imaging, achieving two-photon and wide-field-of-view imaging. In the subsequent year, Zarowny et al. [167] demonstrated a novel GECI with enhanced brightness of the indicator (compared to GCaMP6s) based on a bright monomeric GFP, mNG, in Figure 11C. Calcium dynamic measurement experiments performed in zebrafish larvae proved that the signal-to-noise ratio, kinetics, and baseline brightness of the indicator of mNG were equivalent to those of GCaMP6s (Figure 11D). Zebrafish, distinguished by their transparent bodies and tiny size, are commonly observed for the in vivo imaging of metal ions. Therefore, mNG is expected to be the next generation of GECI. Shemetov et al. [168] incorporated NIR fluorescent proteins into the development of the iGECI sensor, which in combination with NIR Förster resonance energy transfer, enables the iGECI sensors to simultaneously examine neuronal and haemodynamics in the brains of animal models via hybrid photoacoustic and fluorescent microscopy.

#### 5.1.3. $Zn^{2+}$

Intracellular zinc ion disorders are associated with several serious diseases. A two-photon fluorescent probe, CHP-H/CHP-CH3, was designed to monitor the dynamics of zinc ions and HNO (Cyto-JN) in a mouse ischaemia/reperfusion model [169]. The synthesized NIR fluorescent probe could recognize  $Zn^{2+}$  and cyanide, employing the condensation product of isoflurone with p-hydroxybenzaldehyde as the fluorophore while introducing aminourea hydrochloride to increase solubility [170]. The rapid responsiveness (20 s), high sensitivity (detection limit:  $4.61 \times 10^{-8}$  M), and selectivity of this probe led to preliminary confirmation of its  $Zn^{2+}$  and  $CN^-$  logical responses in an animal model.

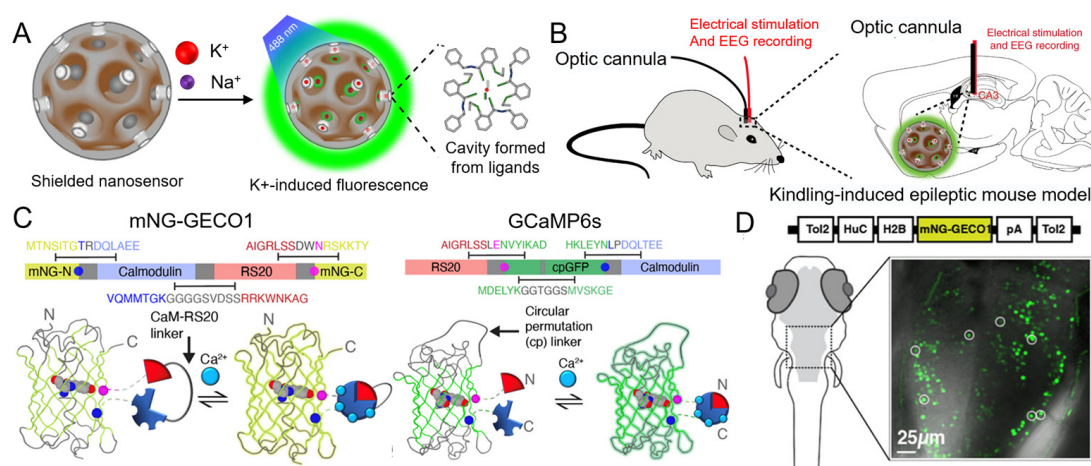


**Figure 11.** Two representative examples of essential metal ion detection in vivo: (A) Schematic showing the design of the  $K^+$  nanosensor. (B) In vivo experimental scheme for  $K^+$  sensing in a kindling-induced epileptic mouse model. Reproduced from [164] with permission from Springer Nature, copyright 2020. (C) Topology and in vitro characterization of mNG-GECO1 and GCaMP6s. (D) Schematic representation of the Tol2[HuC-H2B-mNG-GECO1] construct and confocal image of one fish (5–6 days post fertilization) with 7 regions of interest (ROI) circled. Reproduced from [167] with permission from the American Chemical Society, copyright 2020.

The Lu group modified light-activated DNAzyme on lanthanide-doped UCNP for investigating the distribution of  $Zn^{2+}$  in both cellular and in vivo models [171]. Through the utilization of deeply tissue-penetrating NIR 980 nm light, they were able to achieve spatiotemporal control, providing valuable insights into the dynamic  $Zn^{2+}$  ion distribution. Recently, the same group designed a novel  $Zn^{2+}$  probe based on metal-specific DNAzyme and high-intensity focused ultrasound (HIFU) activation to overcome the problem of spatiotemporal control of metal ion detection, as sketched in Figure 12A [172]. By using a protector strand to block the formation of the catalytic enzyme structure, a  $Zn^{2+}$ -selective DNAzyme probe can be deactivated and, subsequently, reactivated by a HIFU-induced increase in local temperature. This design allows for  $Zn^{2+}$ -specific FRET imaging using the new DNAzyme-HIFU probes, which was successfully demonstrated in both HeLa cells and mice (Figure 12B).

#### 5.1.4. $Fe^{2+}/Fe^{3+}$

The homeostasis of iron ions within human health is of great relevance, as either too high or too low concentrations can cause various systemic diseases. Researchers have worked to achieve ultra-high sensitivity for imaging iron ions in vivo. Vijay et al. developed a rhodamine-B-armed fluorescent chemosensor (RhBNC) that specifically recognizes iron ions and then emits orange fluorescence [173], as shown in Figure 12C. Following photophysical detection, RhBNC was employed for real-time fluorescence imaging in vivo, and bright red fluorescence was observed in the stomach of zebrafish after 30 min of probe treatment with the addition of iron ions (Figure 12D). The carbon dot-based fluorescence sensor has become a representational platform for the detection of iron ions due to its fast response time, low cost, and stability. Chang et al. prepared high quantum yield CDs (42%) by employing a multiflora polygonum one-step hydrothermal strategy and designed a sensor for multicolor imaging [174], tracking intracellular concentration fluctuations, and in vivo bioimaging based on the fluorescence burst of iron ions on CDs. Meanwhile, the same team reported that the fluorescence burst of iron ions on CDs is based on lysis [175]. For the detection of ferrous ions, Zhu et al. combined an NIR strategy to synthesize (E)-4-(2-(3-(dimethylenimino)-5,5-dimethylcyclohexyl-1-en-1-yl)vinyl)-N,N-diethylaniline oxide (DDED) as a NIR probe [176], which showed a strong imaging capability in zebrafish, emitting intense red fluorescence mainly in the yolk sac and digestive tract. DCI-Fe (II),

developed by Zheng et al., allowed for the imaging of ferrous ions within live cell lipid droplets and in mice [177].

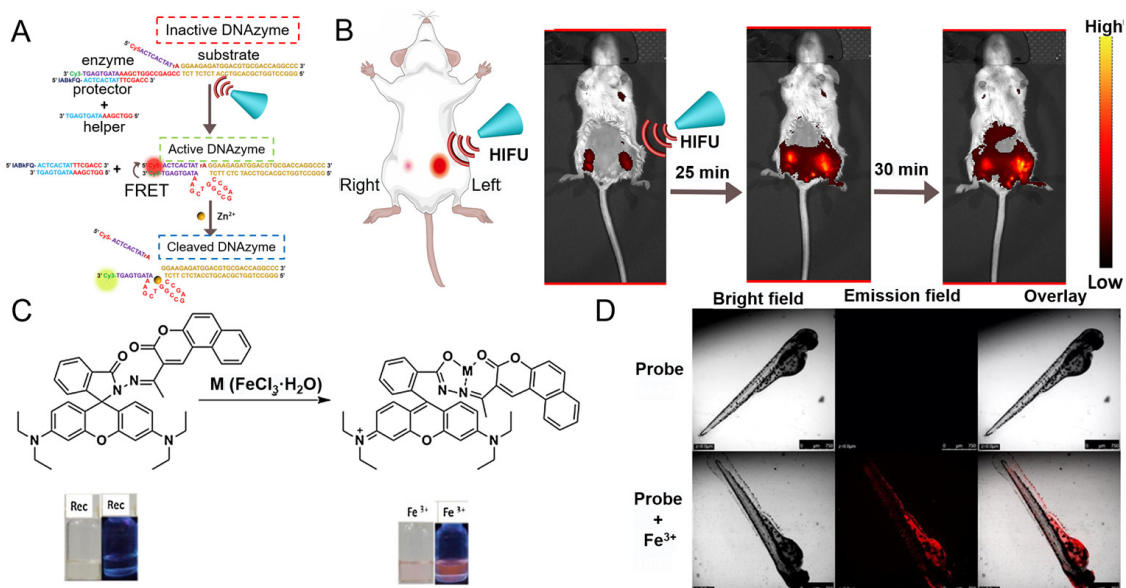


**Figure 12.** Two representative examples of essential metal ion detection in vivo: (A) Schematic of HIFU-activated noninvasive and spatiotemporal control of the DNAzyme-based sensor for Zn<sup>2+</sup> detection in vivo. (B) HIFU-activated metal-ion sensing in vivo. Whole-body fluorescence imaging of mice. Reproduced from [172] with permission from the American Chemical Society, copyright 2022. (C) Proposed sensing mechanism of the probe for the Fe<sup>3+</sup>-sensing event. (D) Confocal fluorescence images of zebrafish embryos (3 days old).

### 5.1.5. Co<sup>2+</sup>

Cobalt is a vital mineral needed in small quantities for DNA biosynthesis and is a key component of vitamin B12. Li's team developed an innovative fluorescent CD sensor using frozen tofu, ethylenediamine, and phosphoric acid [178]. The resulting CD exhibits excellent biocompatibility, high stability, low cytotoxicity, and good water solubility. This sensor can selectively and sensitively detect Co<sup>2+</sup> by fluorescence quenching, with a detection limit of 58 nM. Moreover, strong chelating agents such as EDTA can strip the ions from the surface. In zebrafish models, CD was rapidly absorbed from the intestine to the liver and eliminated from the body within 24 h without significant bioaccumulation.

## 5.2. Fluorescent Sensors for Non-Essential Metal Ions

### 5.2.1. Li<sup>+</sup>

Lithium is prescribed for the treatment of bipolar disorder. The range of 0.6 to 1.2 mM of lithium in serum has been described as clinically safe and therapeutically effective. Over-ingestion of lithium can lead to toxic and even life-threatening reactions [179]. In Figure 13A, Kang et al. reported a fluorescent probe, SP-CE, which was synthesized via introducing an aza-12-crown-4 ether unit into spiropyran for chelation with lithium [180]. In the absence of light, the compound undergoes isomerization from SP to MC form upon complexation with lithium in solution, resulting in a significant fluorescence enhancement upon excitation at 550 nm. The fluorescent probe exhibited high sensitivity and selectivity toward lithium in solution. Finally, it was successfully employed for imaging exogenous lithium in living cells and zebrafish (Figure 13B). Among these, SP-CE has a time-dependent fluorescence response to lithium ions (LiCl treatment) in zebrafish.

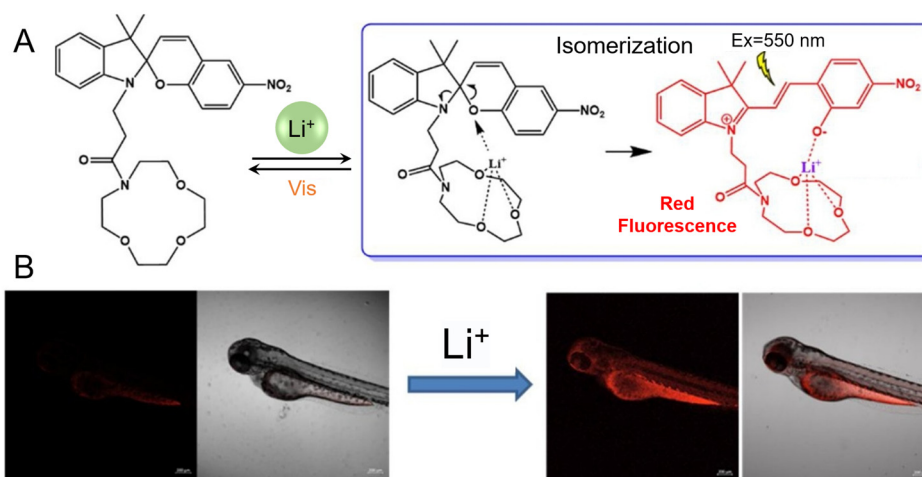


**Figure 13.** (A)  $\text{Li}^+$  fluorescent probe (spirobenzopyrans crowned ether, SP-CE) for in vivo detection of  $\text{Li}^+$ . (B) CLSM images of zebrafish treated by exogenous  $\text{Li}^+$ . Reproduced from [180] with permission from Elsevier, copyright 2019.

### 5.2.2. $\text{Pb}^{2+}$

Huang et al. designed a highly innovative DNAzyme-assembled nanosensor that can sense and image  $\text{Pb}^{2+}$  at NIR light excitation [181]. This nanosensor consists of UCNP as energy transfer donor, BHQ1 quencher as energy transfer acceptor and DNAzyme as  $\text{Pb}^{2+}$  specific pattern of target recognition. Following the introduction of  $\text{Pb}^{2+}$ , the DNAzyme cleaves the strand of substrate at the RNA site, resulting in restoration of luminescence. Imaging data showed that when this nanosensor was micromanipulated into zebrafish embryos, it could image  $\text{Pb}^{2+}$  in living cells and early zebrafish, demonstrating its remarkable potential for in vivo applications.

### 5.2.3. $\text{Sn}^{2+}$

An inadequate  $\text{Sn}^{2+}$  supply can impair hearing and bone growth, while the accumulation of excess can impede zinc metabolism and cause airway and intestinal disorders. A new mitochondria-targeted AIE chemosensor based on naphthoquinone, 2CTA, was synthesized by Palanisamy et al. [182]. Its selectivity and sensitivity (79 nM) to  $\text{Sn}^{2+}$  are higher than those of other disruptors. The “turn-on” fluorescence emission of this chemosensor relies on its AIE properties, caused by the binding of larger aggregates to  $\text{Sn}^{2+}$ . 2CTA selectively aggregates in mitochondria, producing an image merged with MitoTracker Red. It also detected  $\text{Sn}^{2+}$  in zebrafish larvae and responded rapidly within 10 s, making it a promising legal instrument capable of following  $\text{Sn}^{2+}$  in ambient and physical systems.

### 5.2.4. $\text{Cd}^{2+}$

Wang et al. showed that a very simple fluorescent probe (NIS) could be easily prepared by a one-step, one-pot condensation reaction of 2, 3-naphthalenediamine and imidazole-2-carboxaldehyde [183]. In addition, the probe was not disturbed by zinc ions and worked well for  $\text{Cd}^{2+}$  detection at physiological pH. Under fluorescence confocal microscopy, the NIS can detect cadmium ions in living cells through two emission channels. In addition, they further applied NIS to the zebrafish to monitor the real-time uptake of cadmium ions in zebrafish larvae by proportional fluorescence bioimaging.

### 5.2.5. $\text{Hg}^{2+}$

Wu et al. designed and synthesized a coumarin-based reactive fluorescent probe, PIC, for the detection of  $\text{Hg}^{2+}$  [184]. PIC showed greater selectivity for  $\text{Hg}^{2+}$  detection than other metal ions. Specifically, at physiological pH, its fluorescence enhancement for  $\text{Hg}^{2+}$  was 42 times higher than that of other cations. Most importantly, confocal fluorescence

microscopy analysis showed that PIC can be used to monitor  $\text{Hg}^{2+}$  in live cells and zebrafish due to its low cytotoxicity.

#### 5.2.6. $\text{Ni}^{2+}$

The molecular probe based on the nickel-catalyzed deallyl reaction mentioned in the section on nickel ion cell imaging was recently applied to bioimaging in zebrafish. Wang et al. synthesized the probe Ra-Ni by a nucleophilic substitution reaction between rhodamine derivatives and allyl chloride under alkaline conditions [185]. The probe has the advantage of a long wavelength and high tissue permeability, making it suitable for use in live cells and zebrafish for nickel ion imaging.

#### 5.2.7. $\text{Al}^{3+}$

Schiff base ligands with excellent photochemical properties enable the formulation of fluorescent probes with applications in the assay of metal ions [186]. In Figure 14A, Tian et al. developed a high-sensitivity fluorescent probe [187], H3L, which is capable of sensing aluminum ions in living zebrafish, on the basis of a previously designed 2-hydroxynaphthalene Schiff base compound [188]. H3L exhibits blue fluorescence upon exposure to aluminum ions, concentrated in the head and digestive tract of zebrafish (Figure 14B). In particular, blue fluorescence is also observed at the pupil of zebrafish larvae due to the physiological phenomenon of aluminum ion enrichment in their eyes. This probe could be a promising platform for in vivo aluminum ion sensing owing to its high sensitivity and selectivity for the recognition and binding of aluminum ions. Subsequently, the same group improved the 2-hydroxynaphthalene Schiff base fluorescent probe on the basis of modulation in chemical structure [189]. The limit of detection of aluminum ions via this fluorescent probe was enhanced by an order of magnitude ( $10^{-8}$  M) and applied to the in vivo tracing of cells and zebrafish.

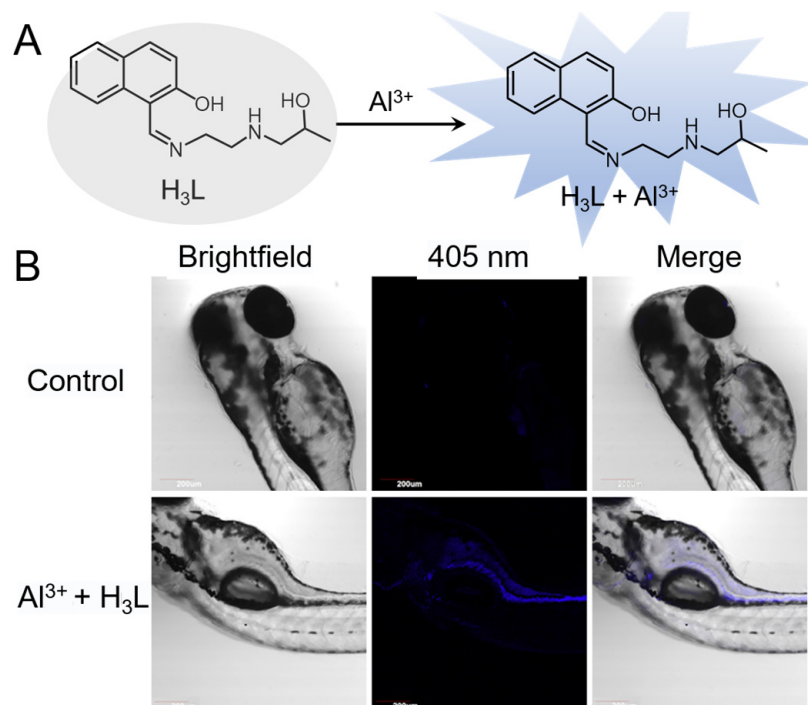


**Figure 14.** (A)  $\text{Al}^{3+}$  fluorescent probe (H3L) for the in vivo detection of  $\text{Al}^{3+}$ . (B) Confocal fluorescence  $\text{Al}^{3+}$  imaging of 3-day-old zebrafish larvae stained with the Schiff base ligand H3L. Reproduced from [186] with permission from Elsevier, copyright 2018.

## 6. Conclusions and Future Directions

In conclusion, this overview highlights the latest advances in fluorescent sensors for metal ion detection in biological systems since 2018. Nucleic acid-based biosensors provide high recognition selectivity and flexible signal transduction mechanisms for the detection of various metal ions. Meanwhile, fluorescent protein-based biosensors are well suited for cellular and *in vivo* imaging. Molecular probes and chemosensors offer the advantages of cost-effectiveness, wide applicability, and ease of manipulation, making them a promising avenue for future development. Nanosensors have revolutionized the field of nanobiosensing with their desirable properties, including high sensitivity, remarkable selectivity, and biocompatibility. Additionally, combining different sensors can amplify their advantages and reduce their disadvantages. For instance, fusion of nucleic acid sensors with nanomaterials can enhance stability and specificity *in vivo*, and conjugation of chemical sensors with nanomaterials can simultaneously improve sensitivity and selectivity in living systems.

Despite the advances in designing fluorescence sensors for metal ion detection in biological systems, there are still challenges to overcome. The detection of a wider range of metal ions is necessary, and there is a need for more sensors for *in vivo* applications. Our future efforts should aim to address the need for improvement in several areas. Specifically, we must focus on improving the toolbox of fluorescent protein-based biosensors and developing more efficient NIR fluorescent proteins with deeper penetration depth, allowing for a significant enhancement of the sensitivity, resolution, and accuracy of *in vivo* metal ion imaging. Additionally, methods need to be developed to ensure the stability of nucleic acid-based biosensors in serum or plasma. The mechanisms of nanosensors must also be better understood, and the water solubility and sensing behavior of water-based systems for chemosensors need to be improved to better detect living systems. These directions must be pursued in parallel to overcome the challenges and improve the effectiveness of fluorescent sensors in detecting metal ions in biological systems. Although there are some difficulties in this field, based on the exciting advances made so far, we expect to develop better sensors in the future, leading to major breakthroughs in biomedical imaging of living systems.

**Funding:** This research was funded by the National Natural Science Foundation of China (no. 22004063, 22274072), Natural Science Foundation of Jiangsu Province (no. 20200303), and State Key Laboratory of Analytical Chemistry for Life Science (5431ZZXM2206).

**Institutional Review Board Statement:** Not applicable.

**Informed Consent Statement:** Not applicable.

**Data Availability Statement:** Not applicable.

**Conflicts of Interest:** The authors declare no conflict of interest.

## Abbreviations

### List of Acronyms

Acronyms	Definition
DNA	Deoxyribonucleic acid
RNA	Ribonucleic acid
ICP-MS	Inductively coupled plasma mass spectrometry
AAS	Atomic absorption spectrophotometry
FAAS	Flame atomic absorption spectrometry
FRET	Fluorescent resonance energy transfer
FNA	Functional nucleic acid
HCR	Hybrid chain reactions
AIE	Aggregation-induced emission
BODIPY	Boron-dipyrromethene

GQ	G-quadruplex
NIR	Near-infrared
CD	Carbon dot
MOF	Metal-organic framework
UV	Ultraviolet
HSA	Human serum albumin
FBS	Fetal bovine serum
PET	Photoinduced electron transfer
SERS	Surface-enhanced Raman scattering
GFP	Green fluorescent protein
TP	Two-photon
AuNP	Gold nanoparticle
GSH	Glutathione
BD	Bipolar disorder
ICT	Intramolecular charge transfer
UNCP	Upconversion nanoparticle
EDTA	Ethylene diamine tetraacetic acid
BHQ	Black hole quencher

## References

- Zoroddu, M.A.; Aaseth, J.; Crisponi, G.; Medici, S.; Peana, M.; Nurchi, V.M. The essential metals for humans: A brief overview. *J. Inorg. Biochem.* **2019**, *195*, 120–129. [[CrossRef](#)] [[PubMed](#)]
- Jomova, K.; Makova, M.; Alomar, S.Y.; Alwasel, S.H.; Nepovimova, E.; Kuca, K.; Rhodes, C.J.; Valko, M. Essential metals in health and disease. *Chem.-Biol. Interact.* **2022**, *367*, 110173. [[CrossRef](#)] [[PubMed](#)]
- Missirlis, F. Regulation and biological function of metal ions in *Drosophila*. *Curr. Opin. Insect Sci.* **2021**, *47*, 18–24. [[CrossRef](#)] [[PubMed](#)]
- Slobodian, M.R.; Petahtegoose, J.D.; Wallis, A.L.; Levesque, D.C.; Merritt, T.J.S. The Effects of Essential and Non-Essential Metal Toxicity in the *Drosophila melanogaster* Insect Model: A Review. *Toxics* **2021**, *9*, 269. [[CrossRef](#)]
- Lu, Y. Metal ions as matchmakers for proteins. *Proc. Natl. Acad. Sci. USA* **2010**, *107*, 1811–1812. [[CrossRef](#)]
- Carter, K.P.; Young, A.M.; Palmer, A.E. Fluorescent Sensors for Measuring Metal Ions in Living Systems. *Chem. Rev.* **2014**, *114*, 4564–4601. [[CrossRef](#)]
- Zhang, X.-B.; Kong, R.-M.; Lu, Y. Metal Ion Sensors Based on DNazymes and Related DNA Molecules. *Annu. Rev. Anal. Chem.* **2011**, *4*, 105–128. [[CrossRef](#)] [[PubMed](#)]
- Chen, Y.; Bai, Y.; Han, Z.; He, W.; Guo, Z. Photoluminescence imaging of Zn<sup>2+</sup> in living systems. *Chem. Soc. Rev.* **2015**, *44*, 4517–4546. [[CrossRef](#)] [[PubMed](#)]
- Zhang, J.; Lu, Y. Biocomputing for Portable, Resettable, and Quantitative Point-of-Care Diagnostics: Making the Glucose Meter a Logic-Gate Responsive Device for Measuring Many Clinically Relevant Targets. *Angew. Chem. Int. Ed.* **2018**, *57*, 9702–9706. [[CrossRef](#)]
- Wu, Z.; Fan, H.; Satyavolu, N.S.R.; Wang, W.; Lake, R.; Jiang, J.-H.; Lu, Y. Imaging Endogenous Metal Ions in Living Cells Using a DNazyme–Catalytic Hairpin Assembly Probe. *Angew. Chem. Int. Ed.* **2017**, *56*, 8721–8725. [[CrossRef](#)]
- Torabi, S.-F.; Wu, P.; McGhee, C.E.; Chen, L.; Hwang, K.; Zheng, N.; Cheng, J.; Lu, Y. In vitro selection of a sodium-specific DNazyme and its application in intracellular sensing. *Proc. Natl. Acad. Sci. USA* **2015**, *112*, 5903–5908. [[CrossRef](#)]
- Hultin, S. *Mosby's Manual of Diagnostic and Laboratory Tests* (4th edn). *Ann. Clin. Biochem.* **2012**, *49*, 415. [[CrossRef](#)]
- Yang, L.; Qing, Z.; Liu, C.; Tang, Q.; Li, J.; Yang, S.; Zheng, J.; Yang, R.; Tan, W. Direct Fluorescent Detection of Blood Potassium by Ion-Selective Formation of Intermolecular G-Quadruplex and Ligand Binding. *Anal. Chem.* **2016**, *88*, 9285–9292. [[CrossRef](#)] [[PubMed](#)]
- Chin, D.; Means, A.R. Calmodulin: A prototypical calcium sensor. *Trends Cell Biol.* **2000**, *10*, 322–328. [[CrossRef](#)]
- Jahnen-Dechent, W.; Ketteler, M. Magnesium basics. *Clin. Kidney J.* **2012**, *5*, i3–i14. [[CrossRef](#)] [[PubMed](#)]
- Maitly, D.; Manna, A.K.; Karthigeyan, D.; Kundu, T.K.; Pati, S.K.; Govindaraju, T. Visible–Near-Infrared and Fluorescent Copper Sensors Based on Julolidine Conjugates: Selective Detection and Fluorescence Imaging in Living Cells. *Chem.-Eur. J.* **2011**, *17*, 11152–11161. [[CrossRef](#)]
- Michielsen, C.M.S.; van Aalen, E.A.; Merckx, M. Ratiometric Bioluminescent Zinc Sensor Proteins to Quantify Serum and Intracellular Free Zn<sup>2+</sup>. *ACS Chem. Biol.* **2022**, *17*, 1567–1576. [[CrossRef](#)]
- Abdolmohammad-Zadeh, H.; Zamani-Kalajahi, M. A turn-on/off fluorescent sensor based on nano-structured Mg-Al layered double hydroxide intercalated with salicylic acid for monitoring of ferric ion in human serum samples. *Anal. Chim. Acta* **2019**, *1061*, 152–160. [[CrossRef](#)]

19. Drennan-Harris, L.R.; Wongwilawan, S.; Tyson, J.F. Trace determination of total mercury in rice by conventional inductively coupled plasma mass spectrometry. *J. Anal. At. Spectrom.* **2013**, *28*, 259–265. [[CrossRef](#)]
20. Xiong, C.; Qin, Y.; Hu, B. On-line separation/preconcentration of V(IV)/V(V) in environmental water samples with CTAB-modified alkyl silica microcolumn and their determination by inductively coupled plasma-optical emission spectrometry. *J. Hazard. Mater.* **2010**, *178*, 164–170. [[CrossRef](#)]
21. Špirić, Z.; Vučković, I.; Stafilov, T.; Kušan, V.; Frontasyeva, M. Air Pollution Study in Croatia Using Moss Biomonitoring and ICP–AES and AAS Analytical Techniques. *Arch. Environ. Contam. Toxicol.* **2013**, *65*, 33–46. [[CrossRef](#)]
22. Wu, P.; He, S.; Luo, B.; Hou, X. Flame Furnace Atomic Absorption Spectrometry: A Review. *Appl. Spectrosc. Rev.* **2009**, *44*, 411–437. [[CrossRef](#)]
23. Săcărescu, L.; Chibac-Scutaru, A.-L.; Roman, G.; Săcărescu, G.; Simionescu, M. Selective detection of metal ions, sulfites and glutathione with fluorescent pyrazolines: A review. *Environ. Chem. Lett.* **2023**, *21*, 561–596. [[CrossRef](#)]
24. Wu, D.; Chen, L.; Lee, W.; Ko, G.; Yin, J.; Yoon, J. Recent progress in the development of organic dye based near-infrared fluorescence probes for metal ions. *Coord. Chem. Rev.* **2018**, *354*, 74–97. [[CrossRef](#)]
25. Denis, M.; Pancholi, J.; Jobe, K.; Watkinson, M.; Goldup, S.M. Chelating Rotaxane Ligands as Fluorescent Sensors for Metal Ions. *Angew. Chem. Int. Ed.* **2018**, *57*, 5310–5314. [[CrossRef](#)] [[PubMed](#)]
26. Liu, X.; Li, N.; Li, M.; Chen, H.; Zhang, N.; Wang, Y.; Zheng, K. Recent progress in fluorescent probes for detection of carbonyl species: Formaldehyde, carbon monoxide and phosgene. *Coord. Chem. Rev.* **2020**, *404*, 213109. [[CrossRef](#)]
27. Wu, L.; Sedgwick, A.C.; Sun, X.; Bull, S.D.; He, X.-P.; James, T.D. Reaction-Based Fluorescent Probes for the Detection and Imaging of Reactive Oxygen, Nitrogen, and Sulfur Species. *Acc. Chem. Res.* **2019**, *52*, 2582–2597. [[CrossRef](#)] [[PubMed](#)]
28. Liu, X.-L.; Niu, L.-Y.; Chen, Y.-Z.; Yang, Y.; Yang, Q.-Z. A multi-emissive fluorescent probe for the discrimination of glutathione and cysteine. *Biosens. Bioelectron.* **2017**, *90*, 403–409. [[CrossRef](#)]
29. Wang, S.-Q.; Wu, Q.-H.; Wang, H.-Y.; Zheng, X.-X.; Shen, S.-L.; Zhang, Y.-R.; Miao, J.-Y.; Zhao, B.-X. Novel pyrazoline-based fluorescent probe for detecting glutathione and its application in cells. *Biosens. Bioelectron.* **2014**, *55*, 386–390. [[CrossRef](#)]
30. Niu, P.; Zhu, J.; Wei, L.; Liu, X. Application of Fluorescent Probes in Reactive Oxygen Species Disease Model. *Crit. Rev. Anal. Chem.* **2022**, *31*, 1–36. [[CrossRef](#)]
31. Cui, W.-L.; Wang, M.-H.; Yang, Y.-H.; Wang, J.-Y.; Zhu, X.; Zhang, H.; Ji, X. Recent advances and perspectives in reaction-based fluorescent probes for imaging peroxynitrite in biological systems. *Coord. Chem. Rev.* **2023**, *474*, 214848. [[CrossRef](#)]
32. Juvekar, V.; Park, S.J.; Yoon, J.; Kim, H.M. Recent progress in the two-photon fluorescent probes for metal ions. *Coord. Chem. Rev.* **2021**, *427*, 213574. [[CrossRef](#)]
33. Wan, H.; Xu, Q.; Gu, P.; Li, H.; Chen, D.; Li, N.; He, J.; Lu, J. AIE-based fluorescent sensors for low concentration toxic ion detection in water. *J. Hazard. Mater.* **2021**, *403*, 123656. [[CrossRef](#)]
34. Xia, P.-F.; Ling, H.; Foo, J.L.; Chang, M.W. Synthetic genetic circuits for programmable biological functionalities. *Biotechnol. Adv.* **2019**, *37*, 107393. [[CrossRef](#)] [[PubMed](#)]
35. Wang, M.; Da, Y.; Tian, Y. Fluorescent proteins and genetically encoded biosensors. *Chem. Soc. Rev.* **2023**, *52*, 1189–1214. [[CrossRef](#)] [[PubMed](#)]
36. Xu, J.; Jiang, R.; Feng, Y.; Liu, Z.; Huang, J.; Ma, C.; Wang, K. Functional nucleic acid-based fluorescent probes for metal ion detection. *Coord. Chem. Rev.* **2022**, *459*, 214453. [[CrossRef](#)]
37. Nagai, T.; Sawano, A.; Park, E.S.; Miyawaki, A. Circularly permuted green fluorescent proteins engineered to sense Ca<sup>2+</sup>. *Proc. Natl. Acad. Sci. USA* **2001**, *98*, 3197–3202. [[CrossRef](#)]
38. Tian, L.; Hires, S.A.; Mao, T.; Huber, D.; Chiappe, M.E.; Chalasani, S.H.; Petreanu, L.; Akerboom, J.; McKinney, S.A.; Schreiter, E.R.; et al. Imaging neural activity in worms, flies and mice with improved GCaMP calcium indicators. *Nat. Methods* **2009**, *6*, 875–881. [[CrossRef](#)] [[PubMed](#)]
39. Torabi, S.-F.; Lu, Y. Functional DNA nanomaterials for sensing and imaging in living cells. *Curr. Opin. Biotechnol.* **2014**, *28*, 88–95. [[CrossRef](#)]
40. Zhou, W.; Saran, R.; Liu, J. Metal Sensing by DNA. *Chem. Rev.* **2017**, *117*, 8272–8325. [[CrossRef](#)]
41. Zhao, L.; Ahmed, F.; Zeng, Y.; Xu, W.; Xiong, H. Recent Developments in G-Quadruplex Binding Ligands and Specific Beacons on Smart Fluorescent Sensor for Targeting Metal Ions and Biological Analytes. *ACS Sens.* **2022**, *7*, 2833–2856. [[CrossRef](#)]
42. Lake, R.J.; Yang, Z.; Zhang, J.; Lu, Y. DNazymes as Activity-Based Sensors for Metal Ions: Recent Applications, Demonstrated Advantages, Current Challenges, and Future Directions. *Acc. Chem. Res.* **2019**, *52*, 3275–3286. [[CrossRef](#)]
43. Li, J.; Mo, L.; Lu, C.-H.; Fu, T.; Yang, H.-H.; Tan, W. Functional nucleic acid-based hydrogels for bioanalytical and biomedical applications. *Chem. Soc. Rev.* **2016**, *45*, 1410–1431. [[CrossRef](#)] [[PubMed](#)]
44. Krämer, J.; Kang, R.; Grimm, L.M.; De Cola, L.; Picchetti, P.; Biedermann, F. Molecular Probes, Chemosensors, and Nanosensors for Optical Detection of Biorelevant Molecules and Ions in Aqueous Media and Biofluids. *Chem. Rev.* **2022**, *122*, 3459–3636. [[CrossRef](#)] [[PubMed](#)]
45. Yang, Y.; Gao, F.; Wang, Y.; Li, H.; Zhang, J.; Sun, Z.; Jiang, Y. Fluorescent Organic Small Molecule Probes for Bioimaging and Detection Applications. *Molecules* **2022**, *27*, 8421. [[CrossRef](#)] [[PubMed](#)]
46. Xu, M.; Xing, J.; Yuan, B.; He, L.; Lu, L.; Chen, N.; Cai, P.; Wu, A.; Li, J. Organic small-molecule fluorescent probe-based detection for alkali and alkaline earth metal ions in biological systems. *J. Mat. Chem. B* **2023**. [[CrossRef](#)]

47. Chen, S.-Y.; Li, Z.; Li, K.; Yu, X.-Q. Small molecular fluorescent probes for the detection of lead, cadmium and mercury ions. *Coord. Chem. Rev.* **2021**, *429*, 213691. [[CrossRef](#)]
48. Lee, H.; Hong, K.-I.; Jang, W.-D. Design and applications of molecular probes containing porphyrin derivatives. *Coord. Chem. Rev.* **2018**, *354*, 46–73. [[CrossRef](#)]
49. Chowdhury, S.; Rooj, B.; Dutta, A.; Mandal, U. Review on Recent Advances in Metal Ions Sensing Using Different Fluorescent Probes. *J. Fluoresc.* **2018**, *28*, 999–1021. [[CrossRef](#)]
50. Raveendran, A.V.; Sankeerthana, P.A.; Jayaraj, A.; Chinna Ayya Swamy, P. Recent developments on BODIPY based chemosensors for the detection of group IIB metal ions. *Results Chem.* **2022**, *4*, 100297. [[CrossRef](#)]
51. Ding, Y.; Zhu, W.-H.; Xie, Y. Development of Ion Chemosensors Based on Porphyrin Analogues. *Chem. Rev.* **2017**, *117*, 2203–2256. [[CrossRef](#)]
52. Pooja Pandey, H.; Aggarwal, S.; Vats, M.; Rawat, V.; Pathak, S.R. Coumarin-based Chemosensors for Metal Ions Detection. *Asian J. Org. Chem.* **2022**, *11*, e202200455. [[CrossRef](#)]
53. Oshchepkov, A.S.; Oshchepkov, M.S.; Oshchepkova, M.V.; Al-Hamry, A.; Kanoun, O.; Kataev, E.A. Naphthalimide-Based Fluorescent Polymers for Molecular Detection. *Adv. Opt. Mater.* **2021**, *9*, 2001913. [[CrossRef](#)]
54. Hazra, A.; Roy, P. A rhodamine based dye for sensing of Group 13 metal ions. *Anal. Chim. Acta* **2022**, *1193*, 339378. [[CrossRef](#)] [[PubMed](#)]
55. Alam, P.; Leung, N.L.C.; Zhang, J.; Kwok, R.T.K.; Lam, J.W.Y.; Tang, B.Z. AIE-based luminescence probes for metal ion detection. *Coord. Chem. Rev.* **2021**, *429*, 213693. [[CrossRef](#)]
56. Vikesland, P.J. Nanosensors for water quality monitoring. *Nat. Nanotechnol.* **2018**, *13*, 651–660. [[CrossRef](#)]
57. Yaari, Z.; Yang, Y.; Apfelbaum, E.; Cupo, C.; Settle, A.H.; Cullen, Q.; Cai, W.; Roche, K.L.; Levine, D.A.; Fleisher, M.; et al. A perception-based nanosensor platform to detect cancer biomarkers. *Sci. Adv.* **2021**, *7*, eabj0852. [[CrossRef](#)] [[PubMed](#)]
58. Kumar, V.; Guleria, P.; Mehta, S.K. Nanosensors for food quality and safety assessment. *Environ. Chem. Lett.* **2017**, *15*, 165–177. [[CrossRef](#)]
59. Auffan, M.; Rose, J.; Bottero, J.-Y.; Lowry, G.V.; Jolivet, J.-P.; Wiesner, M.R. Towards a definition of inorganic nanoparticles from an environmental, health and safety perspective. *Nat. Nanotechnol.* **2009**, *4*, 634–641. [[CrossRef](#)] [[PubMed](#)]
60. Sears, M.E.; Kerr, K.J.; Bray, R.I. Arsenic, Cadmium, Lead, and Mercury in Sweat: A Systematic Review. *J. Environ. Public Health* **2012**, *2012*, 184745. [[CrossRef](#)]
61. Zeng, Z.; Ma, R.; Liu, C.; Xu, Y.; Li, H.; Liu, F.; Sun, S. A crab-like fluorescent probe for Ga(III) detection in body fluids and biological tissues. *Sens. Actuator B-Chem.* **2017**, *250*, 267–273. [[CrossRef](#)]
62. Zheng, P.; Li, M.; Jurevic, R.; Cushing, S.K.; Liu, Y.; Wu, N. A gold nanohole array based surface-enhanced Raman scattering biosensor for detection of silver(i) and mercury(ii) in human saliva. *Nanoscale* **2015**, *7*, 11005–11012. [[CrossRef](#)]
63. Ding, Y.; Tang, Y.; Zhu, W.; Xie, Y. Fluorescent and colorimetric ion probes based on conjugated oligopyrroles. *Chem. Soc. Rev.* **2015**, *44*, 1101–1112. [[CrossRef](#)]
64. Ma, L.; Liu, J. An in Vitro-Selected DNAzyme Mutant Highly Specific for Na<sup>+</sup> under Slightly Acidic Conditions. *ChemBioChem* **2019**, *20*, 537–542. [[CrossRef](#)] [[PubMed](#)]
65. Xiong, Y.; Zhang, J.; Yang, Z.; Mou, Q.; Ma, Y.; Xiong, Y.; Lu, Y. Functional DNA Regulated CRISPR-Cas12a Sensors for Point-of-Care Diagnostics of Non-Nucleic-Acid Targets. *J. Am. Chem. Soc.* **2020**, *142*, 207–213. [[CrossRef](#)]
66. Kaur, G.; Kaur, N. Estimation of sodium ions using easily engineered organic nanoparticles-based turn-on fluorescent sensor: Application in biological and environmental samples. *Sens. Actuator B-Chem.* **2018**, *265*, 134–141. [[CrossRef](#)]
67. Qiao, H.; Bai, J.; Zhang, S.; Li, C. A guanosine-based 2-formylphenylborate ester hydrogel with high selectivity to K<sup>+</sup> ions. *RSC Adv.* **2020**, *10*, 28536–28540. [[CrossRef](#)]
68. Cheng, Y.; Cheng, M.; Hao, J.; Jia, G.; Monchaud, D.; Li, C. The noncovalent dimerization of a G-quadruplex/hemin DNAzyme improves its biocatalytic properties. *Chem. Sci.* **2020**, *11*, 8846–8853. [[CrossRef](#)] [[PubMed](#)]
69. Cheng, Y.; Cheng, M.; Hao, J.; Miao, W.; Zhou, W.; Jia, G.; Li, C. Highly Selective Detection of K<sup>+</sup> Based on a Dimerized G-Quadruplex DNAzyme. *Anal. Chem.* **2021**, *93*, 6907–6912. [[CrossRef](#)] [[PubMed](#)]
70. Chitbankluai, K.; Thavarungkul, P.; Kanatharana, P.; Kaewpet, M.; Buranachai, C. Newly found K<sup>+</sup>-Thioflavin T competitive binding to DNA G-quadruplexes and the development of a label-free fluorescent biosensor with extra low detection limit for K<sup>+</sup> determination in urine samples. *Spectrosc. Acta Part A-Molec. Biomolec. Spectr.* **2022**, *276*, 121244. [[CrossRef](#)]
71. Mazumdar, D.; Nagraj, N.; Kim, H.-K.; Meng, X.; Brown, A.K.; Sun, Q.; Li, W.; Lu, Y. Activity, Folding and Z-DNA Formation of the 8-17 DNAzyme in the Presence of Monovalent Ions. *J. Am. Chem. Soc.* **2009**, *131*, 5506–5515. [[CrossRef](#)] [[PubMed](#)]
72. Xing, S.; Lin, Y.; Cai, L.; Basa, P.N.; Shigemoto, A.K.; Zheng, C.; Zhang, F.; Burdette, S.C.; Lu, Y. Detection and Quantification of Tightly Bound Zn<sup>2+</sup> in Blood Serum Using a Photocaged Chelator and a DNAzyme Fluorescent Sensor. *Anal. Chem.* **2021**, *93*, 5856–5861. [[CrossRef](#)]
73. Chen, F.; Xiao, F.; Zhang, W.; Lin, C.; Wu, Y. Highly Stable and NIR Luminescent Ru-LPMSN Hybrid Materials for Sensitive Detection of Cu<sup>2+</sup> In Vivo. *ACS Appl. Mater. Interfaces* **2018**, *10*, 26964–26971. [[CrossRef](#)] [[PubMed](#)]
74. He, S.-J.; Xie, Y.-W.; Chen, Q.-Y. A NIR-BODIPY derivative for sensing copper(II) in blood and mitochondrial imaging. *Spectrosc. Acta Part A-Molec. Biomolec. Spectr.* **2018**, *195*, 210–214. [[CrossRef](#)]
75. Zheng, W.; Li, H.; Chen, W.; Zhang, J.; Wang, N.; Guo, X.; Jiang, X. Rapid Detection of Copper in Biological Systems Using Click Chemistry. *Small* **2018**, *14*, 1703857. [[CrossRef](#)] [[PubMed](#)]

76. Huang, R.; Xu, Y.; Du, J.; Guan, Q.; Cai, X.; Li, F.; Wang, J.; Chen, W. A fluorescent sensor based on the cascade signal amplification strategy for ultra-sensitive detection of  $\text{Cu}^{2+}$ . *Nanoscale* **2023**, *15*, 1806–1812. [[CrossRef](#)] [[PubMed](#)]
77. Falcone, E.; Gonzalez, P.; Lorusso, L.; Sénèque, O.; Faller, P.; Raibaut, L. A terbium(iii) luminescent ATCUN-based peptide sensor for selective and reversible detection of copper(ii) in biological media. *Chem. Commun.* **2020**, *56*, 4797–4800. [[CrossRef](#)]
78. Flora, K.; Brennan, J.D. Fluorometric Detection of  $\text{Ca}^{2+}$  Based on an Induced Change in the Conformation of Sol–Gel Entrapped Parvalbumin. *Anal. Chem.* **1998**, *70*, 4505–4513. [[CrossRef](#)]
79. Lin, Y.; Zheng, Y.; Guo, Y.; Yang, Y.; Li, H.; Fang, Y.; Wang, C. Peptide-functionalized carbon dots for sensitive and selective  $\text{Ca}^{2+}$  detection. *Sens. Actuator B-Chem.* **2018**, *273*, 1654–1659. [[CrossRef](#)]
80. Zhang, Y.; Yuan, S.; Day, G.; Wang, X.; Yang, X.; Zhou, H.-C. Luminescent sensors based on metal-organic frameworks. *Coord. Chem. Rev.* **2018**, *354*, 28–45. [[CrossRef](#)]
81. Li, W.-Y.; Yang, S.; Li, Y.-A.; Li, Q.-Y.; Guan, Q.; Dong, Y.-B. Synthesis of an MOF-based  $\text{Hg}^{2+}$ -fluorescent probe via stepwise post-synthetic modification in a single-crystal-to-single-crystal fashion and its application in bioimaging. *Dalton Trans.* **2019**, *48*, 16502–16508. [[CrossRef](#)] [[PubMed](#)]
82. Bagheri, M.; Masoomi, M.Y. Sensitive Ratiometric Fluorescent Metal-Organic Framework Sensor for Calcium Signaling in Human Blood Ionic Concentration Media. *ACS Appl. Mater. Interfaces* **2020**, *12*, 4625–4631. [[CrossRef](#)] [[PubMed](#)]
83. Hou, L.; Song, Y.; Xiao, Y.; Wu, R.; Wang, L. ZnMOF-74 responsive fluorescence sensing platform for detection of  $\text{Fe}^{3+}$ . *Microchem. J.* **2019**, *150*, 104154. [[CrossRef](#)]
84. Deng, J.; Hu, J.; Zhao, J.; An, N.; Liang, K.; Wang, Q.; Zhang, Z.; Wu, R.; Zhang, F. Eco friendly synthesis of fluorescent carbon dots for the sensitive detection of ferric ions and cell imaging. *Arab. J. Chem.* **2021**, *14*, 103195. [[CrossRef](#)]
85. Feng, J.; Zhao, X.; Bian, W.; Tang, X. Microwave-assisted synthesis of nitrogen-rich carbon dots as effective fluorescent probes for sensitive detection of  $\text{Ag}^+$ . *Mat. Chem. Front.* **2019**, *3*, 2751–2758. [[CrossRef](#)]
86. Xu, J.; Liu, M.; Zhao, W.; Wang, S.; Gui, M.; Li, H.; Yu, R. DNAzyme-based cascade signal amplification strategy for highly sensitive detection of lead ions in the environment. *J. Hazard. Mater.* **2022**, *429*, 128347. [[CrossRef](#)]
87. Mathivanan, J.; Liu, H.; Gan, J.; Chandrasekaran, A.R.; Sheng, J. Fluorescent Aptaswitch for Detection of Lead Ions. *ACS Appl. Bio Mater.* **2022**, *5*, 5089–5093. [[CrossRef](#)]
88. Shen, G.; Zhang, H.; Xiang, J.; Yang, F.; Wu, S.; Wang, W.; Du, N.; Zhang, J.; Sun, T.; Tang, Y. Direct detection of potassium and lead (II) ions based on assembly-disassembly of a chiral cyanine dye/TBA complex. *Talanta* **2019**, *201*, 490–495. [[CrossRef](#)]
89. Yoon Lee, J.; Kumar Mehta, P.; Subedi, S.; Lee, K.-H. Development of ratiometric fluorescent probes based on peptides for sensing  $\text{Pb}^{2+}$  in aquatic environments and human serum. *Spectrosc. Acta Part A-Molec. Biomolec. Spectr.* **2023**, *294*, 122502. [[CrossRef](#)]
90. Xu, H.; Geng, F.; Jiang, X.; Shao, C.; Wang, Y.; Wang, K.; Qu, P.; Xu, M.; Ye, B.-C. Design of metal-ion-triggered assembly of label-free split G-quadruplex/duplex DNA for turn-on detection of  $\text{Hg}^{2+}$  in fetal calf serum. *Sens. Actuator B-Chem.* **2018**, *255*, 1024–1030. [[CrossRef](#)]
91. Geng, F.; Jiang, X.; Wang, Y.; Shao, C.; Wang, K.; Qu, P.; Xu, M. DNA-based dual fluorescence signals on and ratiometric mercury sensing in fetal calf serum with simultaneous excitation. *Sens. Actuator B-Chem.* **2018**, *260*, 793–799. [[CrossRef](#)]
92. Dey, N. Coordination-driven reversible supramolecular assembly formation at biological pH: Trace-level detection of  $\text{Hg}^{2+}$  and  $\text{I}^-$  ions in real life samples. *Spectrosc. Acta Part A-Molec. Biomolec. Spectr.* **2022**, *267*, 120447. [[CrossRef](#)] [[PubMed](#)]
93. Zhang, Y.; Zhao, Y.; Wu, Y.; Zhao, B.; Wang, L.; Song, B.; Huang, C. Benzoinole-based bifunctional ratiometric turn-on sensor with an ICT effect for trapping of  $\text{H}^+$  and  $\text{Al}^{3+}$  in dual-channel cell imaging and samples. *Spectrosc. Acta Part A-Molec. Biomolec. Spectr.* **2021**, *247*, 119123. [[CrossRef](#)]
94. Chang, M.; Zhang, M.; Hu, H.; Liang, S. Highly selective fluorescence detection of  $\text{Pt}^{4+}$  over  $\text{Pd}^{2+}$  and  $\text{Pt}^{2+}$  using a polyethyleneimine-based nanosensor prepared via facile three-component reaction. *Spectrosc. Acta Part A-Molec. Biomolec. Spectr.* **2022**, *279*, 121466. [[CrossRef](#)] [[PubMed](#)]
95. García-Valle, F.M.; Taberner, V.; Cuenca, T.; Mosquera, M.E.G.; Cano, J. Intramolecular C–F Activation in Schiff-Base Alkali Metal Complexes. *Organometallics* **2019**, *38*, 894–904. [[CrossRef](#)]
96. Ananthan Karthick, K.; Shankar, B.; Kubendran Aravind, M.; Ashokkumar, B.; Tamilselvi, A. Small-Molecule Fluorescent Probe: Ratiometric and Selective Detection of Sodium Ions for Imaging and Solid-State Sensing Applications. *ChemistrySelect* **2022**, *7*, e202203235. [[CrossRef](#)]
97. Deng, Z.; Gao, P.; Liu, H.; He, Y.; Zhong, S.; Yang, Y. Cell-Surface-Anchored DNA Sensors for Simultaneously Monitoring Extracellular Sodium and Potassium Levels. *Anal. Chem.* **2021**, *93*, 16432–16438. [[CrossRef](#)]
98. Ning, J.; Liu, H.; Sun, X.; Song, G.; Shen, M.; Liao, J.; Su, F.; Tian, Y. Rational Design of a Polymer-Based Ratiometric  $\text{K}^+$  Indicator for High-Throughput Monitoring Intracellular  $\text{K}^+$  Fluctuations. *ACS Appl. Bio Mater.* **2021**, *4*, 1731–1739. [[CrossRef](#)] [[PubMed](#)]
99. Pan, T.; Shen, M.; Shi, J.; Ning, J.; Su, F.; Liao, J.; Tian, Y. Intracellular potassium ion fluorescent nanoprobe for functional analysis of hERG channel via bioimaging. *Sens. Actuator B-Chem.* **2021**, *345*, 130450. [[CrossRef](#)]
100. Wang, Z.; Detomasi, T.C.; Chang, C.J. A dual-fluorophore sensor approach for ratiometric fluorescence imaging of potassium in living cells. *Chem. Sci.* **2021**, *12*, 1720–1729. [[CrossRef](#)]
101. Cui, M.-R.; Chen, L.-X.; Li, X.-L.; Xu, J.-J.; Chen, H.-Y. NIR Remote-Controlled “Lock–Unlock” Nanosystem for Imaging Potassium Ions in Living Cells. *Anal. Chem.* **2020**, *92*, 4558–4565. [[CrossRef](#)] [[PubMed](#)]
102. Liu, Z.; Jing, X.; Zhang, S.; Tian, Y. A Copper Nanocluster-Based Fluorescent Probe for Real-Time Imaging and Ratiometric Biosensing of Calcium Ions in Neurons. *Anal. Chem.* **2019**, *91*, 2488–2497. [[CrossRef](#)] [[PubMed](#)]

103. Chen, D.; Zhao, J.; Zhang, L.; Liu, R.; Huang, Y.; Lan, C.; Zhao, S. Capsicum-Derived Biomass Quantum Dots Coupled with Alizarin Red S as an Inner-Filter-Mediated Illuminant Nanosystem for Imaging of Intracellular Calcium Ions. *Anal. Chem.* **2018**, *90*, 13059–13064. [[CrossRef](#)]
104. Pendin, D.; Norante, R.; De Nadai, A.; Gherardi, G.; Vajente, N.; Basso, E.; Kaludercic, N.; Mammucari, C.; Paradisi, C.; Pozzan, T.; et al. A Synthetic Fluorescent Mitochondria-Targeted Sensor for Ratiometric Imaging of Calcium in Live Cells. *Angew. Chem. Int. Ed.* **2019**, *58*, 9917–9922. [[CrossRef](#)]
105. Zhou, W.; Saran, R.; Huang, P.-J.J.; Ding, J.; Liu, J. An Exceptionally Selective DNA Cooperatively Binding Two  $\text{Ca}^{2+}$  Ions. *ChemBioChem* **2017**, *18*, 518–522. [[CrossRef](#)]
106. Li, C.; Chen, P.; Wang, Z.; Ma, X. A DNAzyme-gold nanostar probe for SERS-fluorescence dual-mode detection and imaging of calcium ions in living cells. *Sens. Actuator B-Chem.* **2021**, *347*, 130596. [[CrossRef](#)]
107. Wang, L.; Hiblot, J.; Popp, C.; Xue, L.; Johnsson, K. Environmentally Sensitive Color-Shifting Fluorophores for Bioimaging. *Angew. Chem. Int. Ed.* **2020**, *59*, 21880–21884. [[CrossRef](#)]
108. Zhu, W.; Takeuchi, S.; Imai, S.; Terada, T.; Ueda, T.; Nasu, Y.; Terai, T.; Campbell, R.E. Chemigenetic indicators based on synthetic chelators and green fluorescent protein. *Nat. Chem. Biol.* **2023**, *19*, 38–44. [[CrossRef](#)]
109. van der Linden, F.H.; Mahlandt, E.K.; Arts, J.J.G.; Beumer, J.; Puschhof, J.; de Man, S.M.A.; Chertkova, A.O.; Ponsioen, B.; Clevers, H.; van Buul, J.D.; et al. A turquoise fluorescence lifetime-based biosensor for quantitative imaging of intracellular calcium. *Nat. Commun.* **2021**, *12*, 7159. [[CrossRef](#)] [[PubMed](#)]
110. Wu, P.; Hwang, K.; Lan, T.; Lu, Y. A DNAzyme-Gold Nanoparticle Probe for Uranyl Ion in Living Cells. *J. Am. Chem. Soc.* **2013**, *135*, 5254–5257. [[CrossRef](#)]
111. Li, L.; Feng, J.; Fan, Y.; Tang, B. Simultaneous Imaging of  $\text{Zn}^{2+}$  and  $\text{Cu}^{2+}$  in Living Cells Based on DNAzyme Modified Gold Nanoparticle. *Anal. Chem.* **2015**, *87*, 4829–4835. [[CrossRef](#)] [[PubMed](#)]
112. Yang, C.; Yin, X.; Huan, S.-Y.; Chen, L.; Hu, X.-X.; Xiong, M.-Y.; Chen, K.; Zhang, X.-B. Two-Photon DNAzyme–Gold Nanoparticle Probe for Imaging Intracellular Metal Ions. *Anal. Chem.* **2018**, *90*, 3118–3123. [[CrossRef](#)] [[PubMed](#)]
113. Xiong, M.; Yang, Z.; Lake, R.J.; Li, J.; Hong, S.; Fan, H.; Zhang, X.-B.; Lu, Y. DNAzyme-Mediated Genetically Encoded Sensors for Ratiometric Imaging of Metal Ions in Living Cells. *Angew. Chem. Int. Ed.* **2020**, *59*, 1891–1896. [[CrossRef](#)] [[PubMed](#)]
114. Zhang, X.; Song, Z.-L.; Chao, Q.; Li, Q.; Kong, R.; Fan, G.-C.; Luo, X. A DNAzyme-based normalized fluorescence strategy for direct quantification of endogenous zinc in living cells. *Chem. Commun.* **2022**, *58*, 577–580. [[CrossRef](#)]
115. Yi, D.; Zhao, H.; Zhao, J.; Li, L. Modular Engineering of DNAzyme-Based Sensors for Spatioselective Imaging of Metal Ions in Mitochondria. *J. Am. Chem. Soc.* **2023**, *145*, 1678–1685. [[CrossRef](#)]
116. Zhan, J.; Liu, Z.; Liu, R.; Zhu, J.-J.; Zhang, J. Near-Infrared-Light-Mediated DNA-Logic Nanomachine for Bioorthogonal Cascade Imaging of Endogenous Interconnected MicroRNAs and Metal Ions. *Anal. Chem.* **2022**, *94*, 16622–16631. [[CrossRef](#)]
117. Jayaraj, A.; Gayathri, M.S.; Sivaraman, G.; Swamy, P.C.A. A highly potential acyclic Schiff base fluorescent turn on sensor for  $\text{Zn}^{2+}$  ions and colorimetric chemosensor for  $\text{Zn}^{2+}$ ,  $\text{Cu}^{2+}$  and  $\text{Co}^{2+}$  ions and its applicability in live cell imaging. *J. Photochem. Photobiol. B Biol.* **2022**, *226*, 112371. [[CrossRef](#)]
118. Zhang, G.; Zhao, Y.; Peng, B.; Li, Z.; Xu, C.; Liu, Y.; Zhang, C.; Voelcker, N.H.; Li, L.; Huang, W. A fluorogenic probe based on chelation–hydrolysis–enhancement mechanism for visualizing  $\text{Zn}^{2+}$  in Parkinson’s disease models. *J. Mat. Chem. B* **2019**, *7*, 2252–2260. [[CrossRef](#)]
119. Wang, P.; Wu, X.; Wu, J.; Liao, Y. Highly selective and sensitive peptide-based fluorescent chemosensor for detection of Zinc(II) ions in aqueous medium and living cells. *J. Photochem. Photobiol. A Chem.* **2019**, *382*, 111929. [[CrossRef](#)]
120. Dischler, A.M.; Maslar, D.; Zhang, C.; Qin, Y. Development and Characterization of a Red Fluorescent Protein-Based Sensor RZnP1 for the Detection of Cytosolic  $\text{Zn}^{2+}$ . *ACS Sens.* **2022**, *7*, 3838–3845. [[CrossRef](#)]
121. Murata, O.; Shindo, Y.; Ikeda, Y.; Iwasawa, N.; Citterio, D.; Oka, K.; Hiruta, Y. Near-Infrared Fluorescent Probes for Imaging of Intracellular  $\text{Mg}^{2+}$  and Application to Multi-Color Imaging of  $\text{Mg}^{2+}$ , ATP, and Mitochondrial Membrane Potential. *Anal. Chem.* **2020**, *92*, 966–974. [[CrossRef](#)] [[PubMed](#)]
122. Sadhanala, H.K.; Aryal, S.; Sharma, K.; Orpaz, Z.; Michaeli, S.; Gedanken, A. Nitrogen-doped carbon dots as a highly selective and sensitive fluorescent probe for sensing  $\text{Mg}^{2+}$  ions in aqueous solution, and their application in the detection and imaging of intracellular  $\text{Mg}^{2+}$  ions. *Sens. Actuator B-Chem.* **2022**, *366*, 131958. [[CrossRef](#)]
123. Yadav, N.; Kumar, R.; Singh, A.K.; Mohiyuddin, S.; Gopinath, P. Systematic approach of chromone skeleton for detecting  $\text{Mg}^{2+}$  ion: Applications for sustainable cytotoxicity and cell imaging possibilities. *Spectroc. Acta Part A-Molec. Biomolec. Spectr.* **2020**, *235*, 118290. [[CrossRef](#)]
124. Rane, S.J.; Sivaraman, G.; Pushpalatha, A.M.; Muthusubramanian, S. Quinoline based sensors for bivalent copper ions in living cells. *Sens. Actuator B-Chem.* **2018**, *255*, 630–637. [[CrossRef](#)]
125. Chailek, N.; Kaewnok, N.; Petdum, A.; Sirirak, J.; Chaneam, S.; Kamkaew, A.; Girdthep, S.; Wanichacheva, N. Near infrared and colorimetric fluorescence sensor for ultra-selective detection of  $\text{Cu}^{2+}$  level with applications in diverse water samples, brain tumor cell and flow injection analysis. *J. Photochem. Photobiol. A Chem.* **2021**, *421*, 113533. [[CrossRef](#)]
126. Chang, D.; Shi, L.; Zhang, Y.; Zhang, G.; Zhang, C.; Dong, C.; Shuang, S. Smilax China-derived yellow-fluorescent carbon dots for temperature sensing,  $\text{Cu}^{2+}$  detection and cell imaging. *Analyst* **2020**, *145*, 2176–2183. [[CrossRef](#)] [[PubMed](#)]
127. Wang, Z.; Jia, N.; Zhou, X.; Han, J.; Bu, H. Cu(I)-Catalyzed Click Reaction-Triggered 3D DNA Walker for Constructing an “OFF–ON” Fluorescent Biosensor for  $\text{Cu}^{2+}$  Detection. *ACS Appl. Bio Mater.* **2021**, *4*, 3571–3578. [[CrossRef](#)]

128. Liang, C.; Xie, X.; Shi, Q.; Feng, J.; Zhang, D.; Huang, X. Nitrogen/sulfur-doped dual-emission carbon dots with tunable fluorescence for ratiometric sensing of ferric ions and cell membrane imaging. *Appl. Surf. Sci.* **2022**, *572*, 151447. [[CrossRef](#)]
129. Ge, G.; Li, L.; Chen, M.; Wu, X.; Yang, Y.; Wang, D.; Zuo, S.; Zeng, Z.; Xiong, W.; Guo, C. Green Synthesis of Nitrogen-Doped Carbon Dots from Fresh Tea Leaves for Selective Fe<sup>3+</sup> Ions Detection and Cellular Imaging. *Nanomaterials* **2022**, *12*, 986. [[CrossRef](#)]
130. Cai, H.; Xu, H.; Chu, H.; Li, J.; Zhang, D. Fabrication of multi-functional carbon dots based on “one stone, three birds” strategy and their applications for the dual-mode Fe<sup>3+</sup> detection, effective promotion on cell proliferation and treatment on ferric toxicosis in vitro. *J. Mat. Chem. B* **2021**, *9*, 767–782. [[CrossRef](#)]
131. Diao, Q.; Guo, H.; Yang, Z.; Luo, W.; Li, T.; Hou, D. A rhodamine-6G-based “turn-on” fluorescent probe for selective detection of Fe<sup>3+</sup> in living cells. *Anal. Methods* **2019**, *11*, 794–799. [[CrossRef](#)]
132. Wang, Y.; Liu, F.; Pu, C.; Tong, Z.; Wang, M.; Wang, J. Galactose-imidazole mediated dual-targeting fluorescent probe for detecting Fe<sup>3+</sup> in the lysosomes of hepatocytes: Design, synthesis and evaluation. *Biosens. Bioelectron.* **2022**, *204*, 114083. [[CrossRef](#)] [[PubMed](#)]
133. Rattanopas, S.; Piyanuch, P.; Wisansin, K.; Charoenpanich, A.; Sirirak, J.; Phutdhawong, W.; Wanichacheva, N. Indole-based fluorescent sensors for selective sensing of Fe<sup>2+</sup> and Fe<sup>3+</sup> in aqueous buffer systems and their applications in living cells. *J. Photochem. Photobiol. A Chem.* **2019**, *377*, 138–148. [[CrossRef](#)]
134. McGhee, C.E.; Yang, Z.; Guo, W.; Wu, Y.; Lyu, M.; De Long, C.J.; Hong, S.; Ma, Y.; McInnis, M.G.; O’Shea, K.S.; et al. DNAzyme-Based Lithium-Selective Imaging Reveals Higher Lithium Accumulation in Bipolar Disorder Patient-Derived Neurons. *ACS Central Sci.* **2021**, *7*, 1809–1820. [[CrossRef](#)] [[PubMed](#)]
135. Jiao, Y.; Gao, Y.; Meng, Y.; Lu, W.; Liu, Y.; Han, H.; Shuang, S.; Li, L.; Dong, C. One-Step Synthesis of Label-Free Ratiometric Fluorescence Carbon Dots for the Detection of Silver Ions and Glutathione and Cellular Imaging Applications. *ACS Appl. Mater. Interfaces* **2019**, *11*, 16822–16829. [[CrossRef](#)] [[PubMed](#)]
136. Yu, Q.; Shi, J.; Mudiyansele, A.P.K.K.K.; Wu, R.; Zhao, B.; Zhou, M.; You, M. Genetically encoded RNA-based sensors for intracellular imaging of silver ions. *Chem. Commun.* **2019**, *55*, 707–710. [[CrossRef](#)] [[PubMed](#)]
137. Tang, H.-Y.; Gao, Y.; Li, B.; Li, C.-W.; Guo, Y. Reaction-based colorimetric and ratiometric fluorescent probe for highly selective detection of silver ions. *Sens. Actuator B-Chem.* **2018**, *270*, 562–569. [[CrossRef](#)]
138. Bu, F.; Zhao, B.; Kan, W.; Wang, L.; Song, B.; Wang, J.; Zhang, Z.; Deng, Q.; Yin, G. A phenanthro[9,10-d]imidazole-based AIE active fluorescence probe for sequential detection of Ag<sup>+</sup> / AgNPs and SCN<sup>-</sup> in water and saliva samples and its application in living cells. *Spectrosc. Acta Part A-Molec. Biomolec. Spectr.* **2019**, *223*, 117333. [[CrossRef](#)]
139. Yu, M.; Liu, B.; Guo, J.; Wu, F. A sustainable modificatory 1, 2- alternate thiacalix[4]arene for detection of silver ion. *Dyes Pigment.* **2023**, *210*, 110983. [[CrossRef](#)]
140. Soleja, N.; Mohsin, M. Real time quantification of intracellular nickel using genetically encoded FRET-based nanosensor. *Int. J. Biol. Macromol.* **2019**, *138*, 648–657. [[CrossRef](#)]
141. Wang, X.; Liu, C.; Zhu, H.; Cheng, S.; Zhang, Y.; Su, M.; Rong, X.; Yu, M.; Sheng, W.; Zhu, B. An ultra-sensitive and highly selective fluorescent probe for nickel ions and its environmental and biological applications. *Sens. Actuator B-Chem.* **2022**, *369*, 132300. [[CrossRef](#)]
142. Assiri, M.A.; Junaid, H.M.; Waseem, M.T.; Hamad, A.; Shah, S.H.; Iqbal, J.; Rauf, W.; Shahzad, S.A. AIEE active sensors for fluorescence enhancement based detection of Ni<sup>2+</sup> in living cells: Mechanofluorochromic and photochromic properties with reversible sensing of acid and base. *Anal. Chim. Acta.* **2022**, *1234*, 340516. [[CrossRef](#)] [[PubMed](#)]
143. Gu, Y.-Q.; Shen, W.-Y.; Zhou, Y.; Chen, S.-F.; Mi, Y.; Long, B.-F.; Young, D.J.; Hu, F.-L. A pyrazolopyrimidine based fluorescent probe for the detection of Cu<sup>2+</sup> and Ni<sup>2+</sup> and its application in living cells. *Spectrosc. Acta Part A-Molec. Biomolec. Spectr.* **2019**, *209*, 141–149. [[CrossRef](#)] [[PubMed](#)]
144. Gui, S.; Huang, Y.; Zhu, Y.; Jin, Y.; Zhao, R. Biomimetic Sensing System for Tracing Pb<sup>2+</sup> Distribution in Living Cells Based on the Metal-Peptide Supramolecular Assembly. *ACS Appl. Mater. Interfaces* **2019**, *11*, 5804–5811. [[CrossRef](#)] [[PubMed](#)]
145. Mehta, P.K.; Jeon, J.; Ryu, K.; Park, S.-H.; Lee, K.-H. Ratiometric fluorescent detection of lead ions in aquatic environment and living cells using a fluorescent peptide-based probe. *J. Hazard. Mater.* **2022**, *427*, 128161. [[CrossRef](#)]
146. Wen, J.; Lv, Y.; Xia, P.; Liu, F.; Xu, Y.; Li, H.; Chen, S.-S.; Sun, S. A water-soluble near-infrared fluorescent probe for specific Pd<sup>2+</sup> detection. *Biorg. Med. Chem.* **2018**, *26*, 931–937. [[CrossRef](#)]
147. Wang, D.; Hou, H.; Chen, W.; Wu, Y.; Peng, X.; Song, F. A turn-on fluorescent probe for palladium(II) detection with a large Stokes shift and lysosomes-targeting ability. *Tetrahedron Lett.* **2022**, *102*, 153932. [[CrossRef](#)]
148. Ashwin, B.C.M.A.; Sivaraman, G.; Stalin, T.; Yuvakkumar, R.; Muthu Mareeswaran, P. Selective and sensitive fluorescent sensor for Pd<sup>2+</sup> using coumarin 460 for real-time and biological applications. *J. Photochem. Photobiol. B Biol.* **2018**, *183*, 302–308. [[CrossRef](#)]
149. Zhang, X.-P.; Yuan, Q.; Qi, Y.-L.; Zheng, D.-J.; Liu, Q.-X.; Wang, B.-Z.; Yang, Y.-S.; Zhu, H.-L. An umbelliferone-derived fluorescent sensor for selective detection of palladium(II) from palladium(0) in living cells. *Spectrosc. Acta Part A-Molec. Biomolec. Spectr.* **2019**, *220*, 117134. [[CrossRef](#)]
150. Reagen, S.; Wu, Y.; Liu, X.; Shahni, R.; Bogenschuetz, J.; Wu, X.; Chu, Q.R.; Oncel, N.; Zhang, J.; Hou, X.; et al. Synthesis of Highly Near-Infrared Fluorescent Graphene Quantum Dots Using Biomass-Derived Materials for In Vitro Cell Imaging and Metal Ion Detection. *ACS Appl. Mater. Interfaces* **2021**, *13*, 43952–43962. [[CrossRef](#)]
151. Sun, Y.; Wang, L.; Zhou, J.; Qin, D.; Duan, H. A new phenothiazine-based fluorescence sensor for imaging Hg<sup>2+</sup> in living cells. *Appl. Organomet. Chem.* **2020**, *34*, e5945. [[CrossRef](#)]

152. Zhong, W.; Wang, L.; Qin, D.; Zhou, J.; Duan, H. Two Novel Fluorescent Probes as Systematic Sensors for Multiple Metal Ions: Focus on Detection of Hg<sup>2+</sup>. *ACS Omega* **2020**, *5*, 24285–24295. [[CrossRef](#)] [[PubMed](#)]
153. Ding, G.; Wu, L.; Feng, H.; Liu, Y.; Li, J.; Si, H.; Yao, X.; He, M.; He, W. The specific binding of a new 1,2,3-triazole to three blood proteins and its appended rhodamine complex for selective detection of Hg<sup>2+</sup>. *Spectrosc. Acta Part A-Molec. Biomolec. Spectr.* **2020**, *228*, 117728. [[CrossRef](#)] [[PubMed](#)]
154. Wang, G.; Xu, W.; Liu, Y.; Fu, N. Ultrasensitive detection and high-contrast bioimaging of Hg<sup>2+</sup> using monothiosquaraine-based fluorescent probe via hydrogen bond promoted desulfurization. *Microchem. J.* **2022**, *179*, 107481. [[CrossRef](#)]
155. Lin, W.; Xie, X.; Wang, Y.; Chen, J. A New Fluorescent Probe for Selective Cd<sup>2+</sup> Detection and Cell Imaging. *Z. Anorg. Allg. Chem.* **2019**, *645*, 645–648. [[CrossRef](#)]
156. Wang, P.; An, Y.; Liao, Y. A novel peptide-based fluorescent chemosensor for Cd(II) ions and its applications in bioimaging. *Spectrosc. Acta Part A-Molec. Biomolec. Spectr.* **2019**, *216*, 61–68. [[CrossRef](#)]
157. Guo, Y.; Li, T.; Xie, L.; Tong, X.; Tang, C.; Shi, S. Red pitaya peels-based carbon dots for real-time fluorometric and colorimetric assay of Au<sup>3+</sup>, cellular imaging, and antioxidant activity. *Anal. Bioanal. Chem.* **2021**, *413*, 935–943. [[CrossRef](#)]
158. Bhattacharyya, A.; Makhil, S.C.; Guchhait, N. CHEF-Affected Fluorogenic Nanomolar Detection of Al<sup>3+</sup> by an Anthranilic Acid–Naphthalene Hybrid: Cell Imaging and Crystal Structure. *ACS Omega* **2018**, *3*, 11838–11846. [[CrossRef](#)]
159. Berrones-Reyes, J.; Muñoz-Flores, B.M.; Gómez-Treviño, A.; Treto-Suárez, M.A.; Páez-Hernández, D.; Schott, E.; Zarate, X.; Jiménez-Pérez, V.M. Novel fluorescent Schiff bases as Al<sup>3+</sup> sensors with high selectivity and sensitivity, and their bioimaging applications. *Mater. Chem. Phys.* **2019**, *233*, 89–101. [[CrossRef](#)]
160. Wang, C.-X.; Ai, S.-L.; Wu, B.; Huang, S.-W.; Liu, Z. Biotinylated and fluorophore-incorporated polymeric mixed micelles for tumor cell-specific turn-on fluorescence imaging of Al<sup>3+</sup>. *J. Mat. Chem. B* **2020**, *8*, 3557–3565. [[CrossRef](#)]
161. Fenn, W.O. The Role of Potassium in Physiological Processes. *Physiol. Rev.* **1940**, *20*, 377–415. [[CrossRef](#)]
162. Ning, J.; Lin, X.; Su, F.; Sun, A.; Liu, H.; Luo, J.; Wang, L.; Tian, Y. Development of a molecular K<sup>+</sup> probe for colorimetric/fluorescent/photoacoustic detection of K<sup>+</sup>. *Anal. Bioanal. Chem.* **2020**, *412*, 6947–6957. [[CrossRef](#)] [[PubMed](#)]
163. Liu, J.; Pan, L.; Shang, C.; Lu, B.; Wu, R.; Feng, Y.; Chen, W.; Zhang, R.; Bu, J.; Xiong, Z.; et al. A highly sensitive and selective nanosensor for near-infrared potassium imaging. *Sci. Adv.* **2020**, *6*, eaax9757. [[CrossRef](#)] [[PubMed](#)]
164. Liu, J.; Li, F.; Wang, Y.; Pan, L.; Lin, P.; Zhang, B.; Zheng, Y.; Xu, Y.; Liao, H.; Ko, G.; et al. A sensitive and specific nanosensor for monitoring extracellular potassium levels in the brain. *Nat. Nanotechnol.* **2020**, *15*, 321–330. [[CrossRef](#)]
165. Akerboom, J.; Chen, T.-W.; Wardill, T.J.; Tian, L.; Marvin, J.S.; Mutlu, S.; Calderón, N.C.; Esposti, F.; Borghuis, B.G.; Sun, X.R.; et al. Optimization of a GCaMP Calcium Indicator for Neural Activity Imaging. *J. Neurosci.* **2012**, *32*, 13819. [[CrossRef](#)] [[PubMed](#)]
166. Dana, H.; Sun, Y.; Mohar, B.; Hulse, B.K.; Kerlin, A.M.; Hasseman, J.P.; Tsegaye, G.; Tsang, A.; Wong, A.; Patel, R.; et al. High-performance calcium sensors for imaging activity in neuronal populations and microcompartments. *Nat. Methods* **2019**, *16*, 649–657. [[CrossRef](#)]
167. Zarowny, L.; Aggarwal, A.; Rutten, V.M.S.; Kolb, I.; Patel, R.; Huang, H.-Y.; Chang, Y.-F.; Phan, T.; Kanyo, R.; Ahrens, M.B.; et al. Bright and High-Performance Genetically Encoded Ca<sup>2+</sup> Indicator Based on mNeonGreen Fluorescent Protein. *ACS Sens.* **2020**, *5*, 1959–1968. [[CrossRef](#)]
168. Shemetov, A.A.; Monakhov, M.V.; Zhang, Q.; Canton-Josh, J.E.; Kumar, M.; Chen, M.; Matlashov, M.E.; Li, X.; Yang, W.; Nie, L.; et al. A near-infrared genetically encoded calcium indicator for in vivo imaging. *Nat. Biotechnol.* **2021**, *39*, 368–377. [[CrossRef](#)]
169. Li, M.; Xing, Y.; Zou, Y.; Chen, G.; You, J.; Yu, F. Imaging of the mutual regulation between zinc cation and nitrosyl via two-photon fluorescent probes in cells and in vivo. *Sens. Actuator B-Chem.* **2020**, *309*, 127772. [[CrossRef](#)]
170. Wu, L.; Liu, Y.; Wu, X.; Li, Y.; Du, J.; Qi, S.; Yang, Q.; Xu, H.; Li, Y. A novel Near-Infrared fluorescent probe for Zn<sup>2+</sup> and CN<sup>-</sup> double detection based on dicyanoisfluorone derivatives with highly sensitive and selective, and its application in Bioimaging. *Spectrosc. Acta Part A-Molec. Biomolec. Spectr.* **2022**, *267*, 120621. [[CrossRef](#)]
171. Yang, Z.; Loh, K.Y.; Chu, Y.-T.; Feng, R.; Satyavolu, N.S.R.; Xiong, M.; Nakamata Huynh, S.M.; Hwang, K.; Li, L.; Xing, H.; et al. Optical Control of Metal Ion Probes in Cells and Zebrafish Using Highly Selective DNAzymes Conjugated to Upconversion Nanoparticles. *J. Am. Chem. Soc.* **2018**, *140*, 17656–17665. [[CrossRef](#)]
172. Wang, X.; Kim, G.; Chu, J.L.; Song, T.; Yang, Z.; Guo, W.; Shao, X.; Oelze, M.L.; Li, K.C.; Lu, Y. Noninvasive and Spatiotemporal Control of DNAzyme-Based Imaging of Metal Ions In Vivo Using High-Intensity Focused Ultrasound. *J. Am. Chem. Soc.* **2022**, *144*, 5812–5819. [[CrossRef](#)] [[PubMed](#)]
173. Vijay, N.; Wu, S.P.; Velmathi, S. Turn on fluorescent chemosensor containing rhodamine B fluorophore for selective sensing and in vivo fluorescent imaging of Fe<sup>3+</sup> ions in HeLa cell line and zebrafish. *J. Photochem. Photobiol. A Chem.* **2019**, *384*, 112060. [[CrossRef](#)]
174. Chang, D.; Zhao, Z.; Niu, W.; Shi, L.; Yang, Y. Iron ion sensing and in vitro and in vivo imaging based on bright blue-fluorescent carbon dots. *Spectrosc. Acta Part A-Molec. Biomolec. Spectr.* **2021**, *260*, 119964. [[CrossRef](#)] [[PubMed](#)]
175. Chang, D.; Zhao, Z.; Shi, L.; Liu, W.; Yang, Y. Lysosome-targeted carbon dots for colorimetric and fluorescent dual mode detection of iron ion, in vitro and in vivo imaging. *Talanta* **2021**, *232*, 122423. [[CrossRef](#)] [[PubMed](#)]
176. Zhu, M.; Zhao, Z.; Liu, X.; Chen, P.; Fan, F.; Wu, X.; Hua, R.; Wang, Y. A novel near-infrared fluorimetric method for point-of-care monitoring of Fe<sup>2+</sup> and its application in bioimaging. *J. Hazard. Mater.* **2021**, *406*, 124767. [[CrossRef](#)] [[PubMed](#)]
177. Zheng, J.; Feng, S.; Gong, S.; Xia, Q.; Feng, G. In vivo imaging of Fe<sup>2+</sup> using an easily obtained probe with a large Stokes shift and bright strong lipid droplet-targetable near-infrared fluorescence. *Sens. Actuator B-Chem.* **2020**, *309*, 127796. [[CrossRef](#)]

178. Wen, X.; Wen, G.; Li, W.; Zhao, Z.; Duan, X.; Yan, W.; Trant, J.F.; Li, Y. Carbon dots for specific “off-on” sensing of  $\text{Co}^{2+}$  and EDTA for in vivo bioimaging. *Mater. Sci. Eng. B* **2021**, *123*, 112022. [[CrossRef](#)]
179. Stubing, D.B.; Heng, S.; Abell, A.D. Crowned spiropyran fluoroionophores with a carboxyl moiety for the selective detection of lithium ions. *Org. Biomol. Chem.* **2016**, *14*, 3752–3757. [[CrossRef](#)]
180. Kang, J.; Li, E.; Cui, L.; Shao, Q.; Yin, C.; Cheng, F. Lithium ion specific fluorescent reversible extraction-release based on spiropyran isomerization combining crown ether coordination and its bioimaging. *Sens. Actuator B-Chem.* **2021**, *327*, 128941. [[CrossRef](#)]
181. Huang, L.; Chen, F.; Zong, X.; Lu, Q.; Wu, C.; Ni, Z.; Liu, M.; Zhang, Y. Near-infrared light excited UCNPs-DNAzyme nanosensor for selective detection of  $\text{Pb}^{2+}$  and in vivo imaging. *Talanta* **2021**, *227*, 122156. [[CrossRef](#)] [[PubMed](#)]
182. Ravichandiran, P.; Prabakaran, D.S.; Maroli, N.; Boguszewska-Czubara, A.; Maslyk, M.; Kim, A.R.; Kolandaivel, P.; Ramalingam, P.; Park, B.-H.; Han, M.-K.; et al. Mitochondria-targeted dual-channel colorimetric and fluorescence chemosensor for detection of  $\text{Sn}^{2+}$  ions in aqueous solution based on aggregation-induced emission and its bioimaging applications. *J. Hazard. Mater.* **2021**, *415*, 125593. [[CrossRef](#)]
183. Wang, J.H.; Liu, Y.M.; Chao, J.B.; Wang, H.; Wang, Y.; Shuang, S. A simple but efficient fluorescent sensor for ratiometric sensing of  $\text{Cd}^{2+}$  and bio-imaging studies. *Sens. Actuator B-Chem.* **2020**, *303*, 127216. [[CrossRef](#)]
184. Chen, C.-G.; Vijay, N.; Thirumalaivasan, N.; Velmathi, S.; Wu, S.-P. Coumarin-based  $\text{Hg}^{2+}$  fluorescent probe: Fluorescence turn-on detection for  $\text{Hg}^{2+}$  bioimaging in living cells and zebrafish. *Spectrosc. Acta Part A-Molec. Biomolec. Spectr.* **2019**, *219*, 135–140. [[CrossRef](#)]
185. Wang, X.; Cheng, S.; Liu, C.; Zhang, Y.; Su, M.; Rong, X.; Zhu, H.; Yu, M.; Sheng, W.; Zhu, B. A novel ratiometric fluorescent probe for the detection of nickel ions in the environment and living organisms. *Sci. Total Environ.* **2022**, *840*, 156445. [[CrossRef](#)] [[PubMed](#)]
186. Tai, A.W.; Lien, E.J.; Lai, M.M.C.; Khwaja, T.A. Novel N-hydroxyguanidine derivatives as anticancer and antiviral agents. *J. Med. Chem.* **1984**, *27*, 236–238. [[CrossRef](#)]
187. Tian, H.; Qiao, X.; Zhang, Z.-L.; Xie, C.-Z.; Li, Q.-Z.; Xu, J.-Y. A high performance 2-hydroxynaphthalene Schiff base fluorescent chemosensor for  $\text{Al}^{3+}$  and its applications in imaging of living cells and zebrafish in vivo. *Spectrosc. Acta Part A-Molec. Biomolec. Spectr.* **2019**, *207*, 31–38. [[CrossRef](#)]
188. Lian, W.-J.; Wang, X.-T.; Xie, C.-Z.; Tian, H.; Song, X.-Q.; Pan, H.-T.; Qiao, X.; Xu, J.-Y. Mixed-ligand copper(II) Schiff base complexes: The role of the co-ligand in DNA binding, DNA cleavage, protein binding and cytotoxicity. *Dalton Trans.* **2016**, *45*, 9073–9087. [[CrossRef](#)]
189. Wang, Q.; Yang, L.; Wang, H.; Song, J.; Ding, H.; Tang, X.-H.; Yao, H. A highly selective and sensitive turn-on fluorescent probe for the detection of  $\text{Al}^{3+}$  and its bioimaging. *Luminescence* **2017**, *32*, 779–785. [[CrossRef](#)] [[PubMed](#)]

**Disclaimer/Publisher’s Note:** The statements, opinions and data contained in all publications are solely those of the individual author(s) and contributor(s) and not of MDPI and/or the editor(s). MDPI and/or the editor(s) disclaim responsibility for any injury to people or property resulting from any ideas, methods, instructions or products referred to in the content.